# Crystallographic and Seismic Anisotropies of Calcite at Different Depths: A Study Using Quantitative Texture Analysis by Neutron Diffraction

**Michele Zucali [1,2], Daniel Chateigner [3] and Bachir Ouladdiaf [4]**

[1]   Dipartimento di Scienze della Terra - Università degli Studi di Milano, Italy; michele.zucali@unimi.it
[2]   Department of Earth and Atmospheric Sciences - University of Houston, Texas - USA; mzucali@uh.edu
[3]   Laboratoire de Cristallographie et Sciences des Matériaux (CRISMAT), Ecole Nationale Supérieure d'Ingénieurs de Caen University of CAEN - France; daniel.chateigner@ensicaen.fr
[4]   Institut Laue-Langevin - 71 avenue des Martyrs CS 20156, 38042 Grenoble Cedex 9 - France; ouladdiaf@ill.eu
*    Correspondence: michele.zucali@unimi.it

**Abstract:**   Eight samples of limestones and marbles were studied by neutron diffraction to collect Quantitative Texture (i.e., Crystallographic Preferred Orientations or CPO) of calcite deforming at different depths in the crust. We studied the different Texture patterns developed in shear zones at different depth and their influence on seismic anisotropies. Samples were collected in the French and Italian Alps, Apennines, and Paleozoic Sardinian basement. They are characterized by isotropic to highly anisotropic (e.g., mylonite shear zone) fabrics. Mylonite limestones occur as shear zone horizons within the Cenozoic Southern Domain in Alpine thrust-and-fold belts (Italy), the Briançonnais domain of the Western Alps (Italy-France border), the Sardinian Paleozoic back-thrusts or in the Austroalpine intermediate units. The analyzed marbles were collected in the Carrara Marble, in the Austroalpine Units in the Central (Mortirolo) and Western Alps (Valpelline). The temperature and depth of development of fabrics vary from < 100°C, to 800°C and depth from <10 km to about 30 km, corresponding from upper to lower crust conditions. Quantitative Texture Analysis shows different types of patterns for calcite: random to strongly textured. Textured types may be further separated in orthorhombic and monoclinic (Types A and B), based on the angle defined with the mesoscopic fabrics. Seismic anisotropies were calculated by homogenizing the single crystal elastic tensor, using the Orientation Distribution Function calculated by the Quantitative Texture Analysis. The resulting P- and S-waves anisotropies show a wide variability due to the textural types, temperature and pressure conditions, and dip of the shear planes.

**Keywords:** calcite; seismic anisotropy; texture; CPO; thrust; shear zone; neutron diffraction; crust

## 1. Introduction

The quantification of the seismic response of rocks is a fundamental task in understanding Earth's structure, from the core to the surface [1]. The large-scale seismic experiments, now with high-resolution arrays, is the most used approach to image the Earth and to resolve the distribution of natural resources in-depth, e.g. water, ore minerals, and oil & gas [2,3]. However, the interpretation of seismic images strongly relies on the knowledge of seismic response of the anisotropic aggregates of minerals composing the rocks, which in turn is intimately related to the textures of rocks [4], as well as on their extrinsic shape preferred features [5]. In the last two decades, a great effort has been made to quantify the seismic response

of natural aggregates, chiefly by using the 2-Dimensional approach of the EBSD (Electron Back Scattered Diffraction) to reconstruct the Orientation Distribution Function (e.g. [6–8]). Carbonate rocks occur at the Earth's surface and upper crust levels, as sedimentary cover, but can be found within the intermediate and lower crust, as marbles. Within the upper crust, the tectonic deformation often localizes within carbonate rocks, producing thrust-folds systems [9,10]. Though less diffuse within the metamorphic basements, carbonate rocks are known to be equally crucial at depth because they likely represent weak horizons, often separating tectonometamorphic units [11,12]. For these reasons, the knowledge of the texture and seismic response of carbonate rocks is essential to interpret seismic anisotropy at various depth within the crust [13]. Several works have been dedicated to study the behavior of calcite single crystal, limestones, and marbles at different temperature and pressure [14–19]. A general scheme of the expected textures has been developed, combining natural and numerical data (see [20] and references therein), but data are still needed. Moreover, virtually no work has been dedicated to combining the neutron diffraction textural data with the prediction of seismic velocities through the homogenization of the elastic tensor [21,22].

With this contribution, we aim at producing new data related to the textures of carbonate rocks. In particular, we aim at relating different pressure, temperature, and shear geometry conditions of deformation with the type of texture developed. We also aim at investigating the control of texture types on the seismic anisotropies. The presented study will hence provide a reference to interpret measured seismic anisotropy in the continental crust [23], where carbonate rocks might be also involved in accommodating shearing along mylonitic horizons.

For this aim, we selected carbonate rocks characterized by fabrics developed at different temperature and pressure conditions and different strain geometries, from pure to simple shear, representing some of the large number of possible combinations in naturally deformed rocks. The samples have been collected mainly in the Alpine system and display a various degree of planar fabrics, developed at different depths within the crust. In this contribution, we will produce new texture data to be included in the general scheme of texture development. Moreover, we will calculate the component of the seismic anisotropies due to the texture by homogenizing the stiffness tensor using the Orientation Distribution Function obtained with the Quantitative Texture Analysis. Finally, we will investigate the influence of the orientation of the foliation plane on the seismic anisotropy [24] at different depth in the crust and with different textures.

## 2. Samples description and geological setting

Samples were collected in the French and Italian Alps, Apennines, and Paleozoic basement (Figure 1). Different locations (Figure 1) were chosen to sample carbonate rocks from different crustal levels, from upper/intermediate crust limestones to lower crust high-temperature marbles (Table 1).

According to Figure 1, upper crust samples were collected in the Southalpine domain, Sardinia and Helvetic-Dauphinoise (e.g., Triassic and Jurassic limestones). All samples preserve at macroscopic scale their primary features; intermediate crust samples were collected in the Briançonnais domain and in the Central Austroalpine domain, where Mesozoic sediments were involved in the Alpine tectonics at relatively upper levels. However, they still preserve their stratigraphic relations with the surrounding rocks, as sedimentary strata or laminations. The last group of samples, collected in the Carrara metamorphic complex, and in the Western-Central Austroalpine domain, are metamorphic marbles. In this last group, no sedimentary features are preserved.

- The BAS sample is a light gray crystalline limestone, fine-grained, homogeneous, and free of any planar fabrics at the macroscopic scale, both primary or secondary, as fractures or joints. It is Jurassic in age and it belongs to the External thrust-belt French Subalpine system [25,26]; it is part of the so-called Calcaires "tithoniques" [27]. It was sampled close to Grenoble (France), La Bastille, the southernmost part of the Chartreuse massive. According to the tectonic reconstruction and the local

geologic map [27,28], the thrust system developed a km-scale anticline, associated with brittle faults and fracture systems. The BAS sample has been collected within this anticline but far from the brittle system. The fold and thrust system occurred at < 3km depth, at temperature <100°C.

- The SOD sample was collected in the Southalpine domain. The sample is part of the Triassic cover, which crops along the entire Southalpine domain. The general interpretation infers the thrust and fold system to convergent tectonics active during the formation of the Alpine system (Figures 1 and 2). It was collected within the meter-scale mylonitic horizons associated with a meter to tens of meters asymmetric folds [29]. According to these authors, the thrust horizons occurred at relatively upper depth, not exceeding 5-7 km, corresponding to a maximum of 200°C. The studied sample shows an abrupt change in fabric from undeformed to highly strained domains (Figure 2), often associated with grain-size reduction, pressure-solution, and plastic deformation in carbonate grains, testified by mechanical twinning. These meso- and microstructures support temperatures as high as 200°C [30,31]. The kinematics of these thrust horizons have been reconstructed based on stratigraphic and structural constraints, being characterized by strong simple shear components also testified by classical shear indicators, as cm- to mm-scale drag folds and porphyroclasts geometries [32].

- SA1 sample was collected in the Sardinia basement. It is part of the Ceroidi Limestone (Gonnesa Fm.), pre-Ordovician protolith of the External Zone. This metasedimentary cover has been deeply involved in the Paleozoic-Variscan tectonics [33]. During the Variscan tectonic activity green-schists metamorphic conditions were attained [34], locally associated with high strain shear horizons, from meters to tens of meters thick [35,36]. The SA1 sample was collected in one of these high strain horizons, made by meta-carbonate limestone. The Variscan deformation developed as pervasive folding systems. However, the SA1 sample was collected far from folds and within the domain where the mylonitic foliation is well visible at macroscopic scale (Figure 2). As qualitative estimates for pressure and temperature, the intermediate limit can be put following the metamorphic evolution of the inner part of the belt, as described by Elter et al [37]. Consequently, a limit of 350°C and 4-5 kbar, corresponding to roughly 12-15 km depth can be used to constrain the development of the fabric in this horizon. Moreover, mesoscopically no asymmetric shear sense indicators have been recognized, supporting the microstructural and textural observations [35], which suggested a pure shear strain.

- STE sample was collected in the Central Alps, within the intermediate Austroalpine domain [38]. Here the Mesozoic sedimentary cover was involved in the Alpine tectonics, occurring as thick-skinned thrusting of cover and its pre-alpine basement [39]. Thrusting localized along high strain horizons within cover and basement [40]. The temperature conditions of this event were estimated at T=300-350°C at depth=15-20km [41,42]. We collected a sample within the mylonite horizons in the Mesozoic cover, namely the Fraele Fm. It is characterized by a strongly developed mylonite fabric, associated with a meter- to tens of meter folds. A strong transposition of the lithostratigraphic features has been recorded along this horizon [43]. A simple shear component has been described for this deformation based on meso- and microstructural analysis [41]. Sample scale features, as mm-sized drag faults (Figure 2), support the simple shear component.

- CC sample was collected in the Western Alps, in the sub-Briançonnais domain. It consists of Jurassic limestone strongly deformed during Alpine thrusting of the external part of the chain [44]. According to [45,46] the External Briançonnais units equilibrated at pressure not exceeding 5 kbar, corresponding to depth <15 km, and T=300-350 °C. Moreover, an overall simple shear kinematics is constrained by map- to micro-scale indicators, extensively described in the area [47–49]; however, the studied sample does not show clear microstructures that could be uniquely related to a simple shear geometry (Figure 2).

- P1 was collected in the well-known Carrara marbles quarries. They consist of Mesozoic cover of the Autochthon of the Tuscan Units metamorphosed during the Alpine evolution [50,51]. Km- to

119  meter-scale folding systems have been mapped, and several kinematics reconstructions have been
120  proposed [52] suggesting large scale shear, related to the thrusting of the deep units, resulted in
121  meso- and micro-scale simple shear fabrics (e.g. [20,53]). However, large scale strain partitioning also
122  occurred, allowing large volume of marbles to escape the development of planar or linear fabrics [54].
123  In fact, the studied sample is characterized by isotropic equigranular texture of recrystallized calcite
124  (Figure 2), suggesting a static recrystallization process associated with grain-boundary migration
125  both leading to grainsize increase [32]. Within the Alpi Apuane Metamorphic Complex the estimated
126  conditions of metamorphism point to T=400-500°C at 8-10kbar [50,55,56], corresponding to 25-30 km
127  depth.

128 • VP3 and MA1 were both collected in the Austroalpine domain of the Alps [44]. The Austroalpine
129  domain is interpreted as fragments of the pre-alpine continental crust involved in the Alpine
130  subduction-collision system. The collected samples are marbles whose metamorphism has produced
131  during high-temperature Permian-Triassic extension [57]. VP3 was collected in the Valpelline
132  Series, Austroalpine of the Western Alps [58,59], while MA1 was collected in the Languard-Campo,
133  Austroalpine domain of the Central Alps [60]. They are characterized by 0.5-1.5 mm (VP3) to <0.5
134  mm (MA1) grain-size and a strong planar fabric, marked by the shape preferred orientation of
135  calcite and local diopside and quartz (Figure 2). They display diffuse mechanical twinning and
136  undulose extinction, both suggesting grain-scale plastic deformation [32]. Shear indicators are not
137  univocal, MA1 often shows asymmetrical bending of calcite tails around porphyroblast suggesting a
138  component of simple shear, but pure shear cannot be ruled out. Similarly, VP3 displays a less tendency
139  to develop asymmetric microstructures, point to a greater contribution of pure shear. Metamorphic
140  conditions have been quantitatively determined for both samples, VP3 developed at T=700-800°C and
141  P>6kbar, corresponding to >18km depth, while MA1 fabric was estimated to form at T=600-750°C
142  and P=6.5-7.5kbar, corresponding to 20-24km depth [58,60].
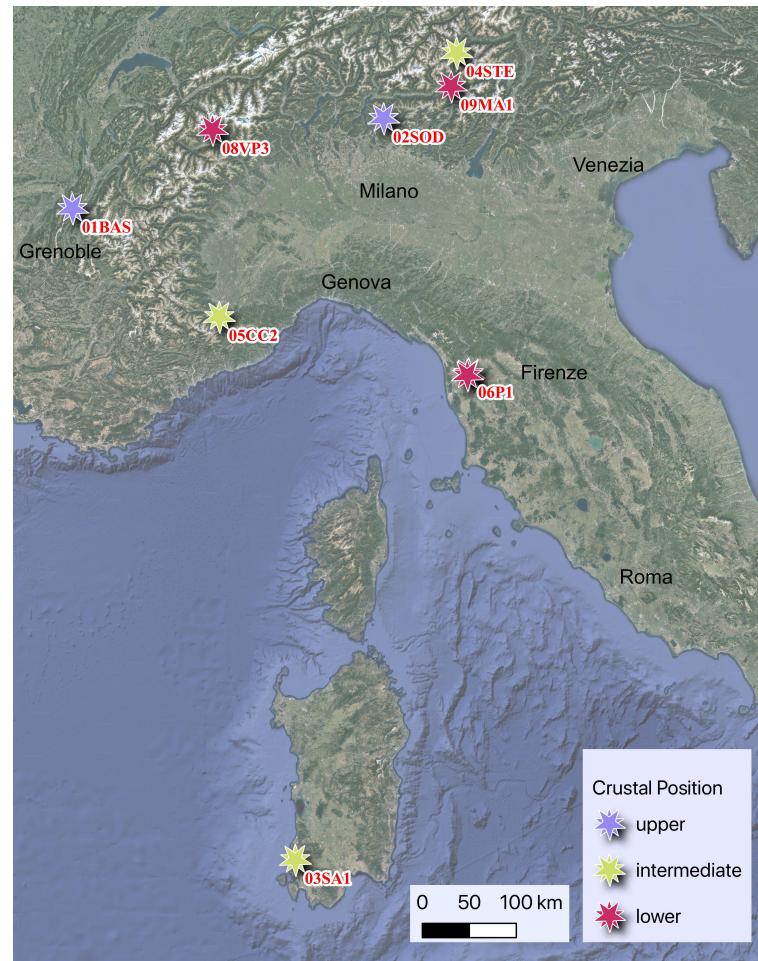
**Figure 1.** Location and crustal position of the studied samples, see text for explanation

**Table 1.** List of samples labels with Alpine geological domain, crustal position with depth in km, temperature in °C and shear geometry. Labels are the same as used in figures and text. See text for references on P, T and shear geometry. **Upper crust** for depth <10km at T < 300°C, **intermediate crust** for depth between 10 and 20km and T between 300 and 400 °C, and **lower crust** for depth >20km and T> 400°C

| Label | Domain | Crustal Position | Temperature | shear geometry |
|-------|--------|------------------|-------------|----------------|
| 01BAS | Helvetic-Dauphinoise | upper (<3km) | <100°C | no shear |
| 02SOD | Southalpine | upper (<5-7km) | ≈200°C | simple shear |
| 03SA1 | Sardinia Basement | intermediate (12-15km) | ≈350°C | pure shear |
| 04STE | Austroalpine | intermediate (15-20km) | 300-350°C | simple shear |
| 05CC2 | Briançonnaise | intermediate (<15km) | 300-350°C | pure/simple shear |
| 06P1 | Apuane Metamorphic Complex | lower (25-30km) | 400-500°C | no shear |
| 08VP3 | Austroalpine | lower (>18/20km) | 700-800°C | pure/simple shear |
| 09MA1 | Austroalpine | lower (20-24km) | 600-750°C | simple/pure shear |
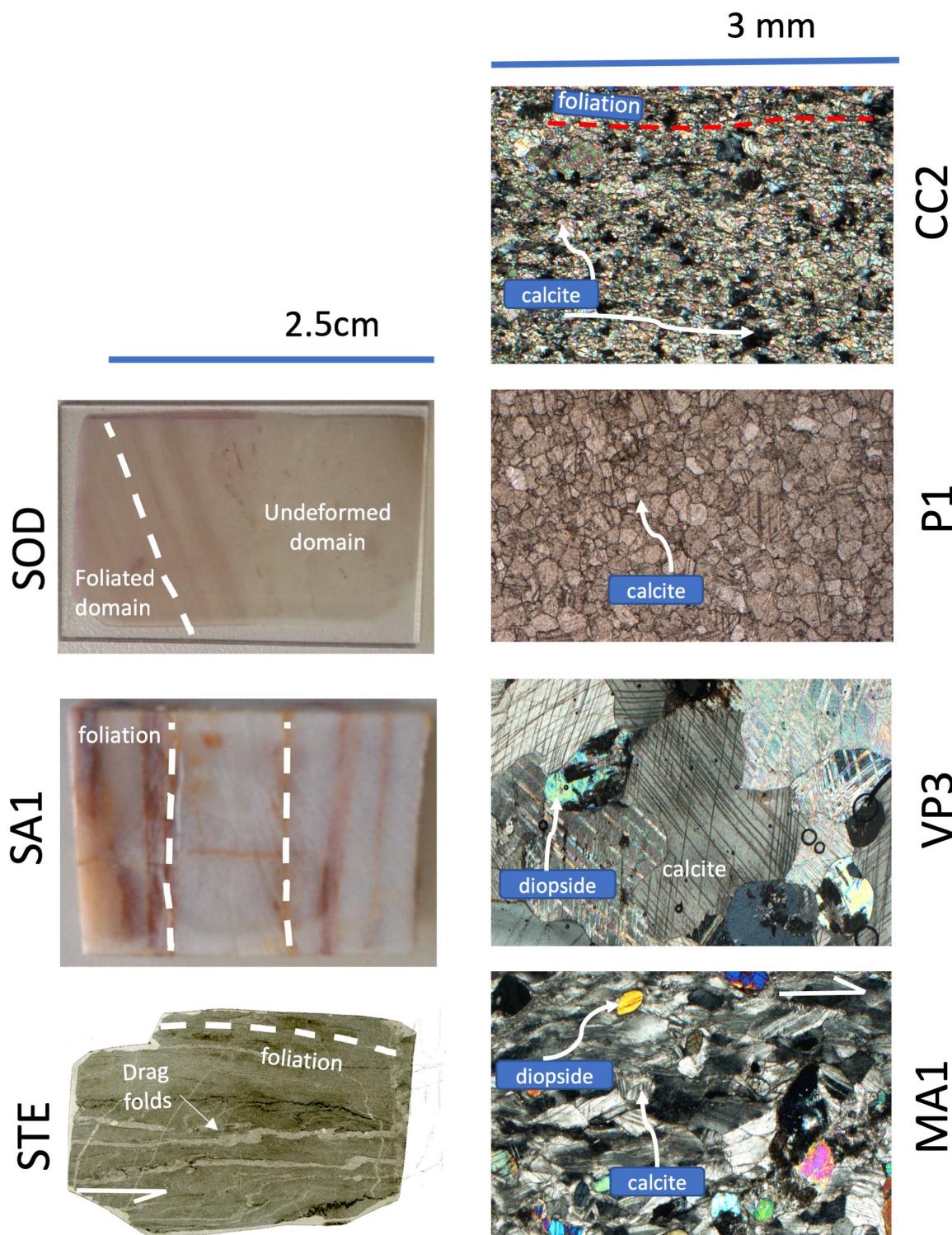
**Figure 2.** Images of selected samples showing main fabric features as layering or foliation. Scale is indicated. Long side of the image 2.5 cm for STE, SA1 and SOD; long side of the image is 3.0 mm for MA1, VP3, P1 and CC2. MA1, VP3 and CC2 images with crossed polarizers. P1 image with plane polarizers.

### 3. Sample Reference System and Methods

The samples were cut in cubes of ≈ 1cm edge (Figure 3); the three axes of the cube correspond to the orthonormal reference of the sample. In this orthogonal Sample Reference System, the plane XY corresponds to the stratification or shear plane, while X direction is taken parallel to the flow direction or lineation, if it exists (Figure 3). The references in figure 3b are used in all the Pole Figures (Figures 4, 5, 6). Pole figures display pole densities in multiples of a uniform distribution (mud).

## Sample Reference System
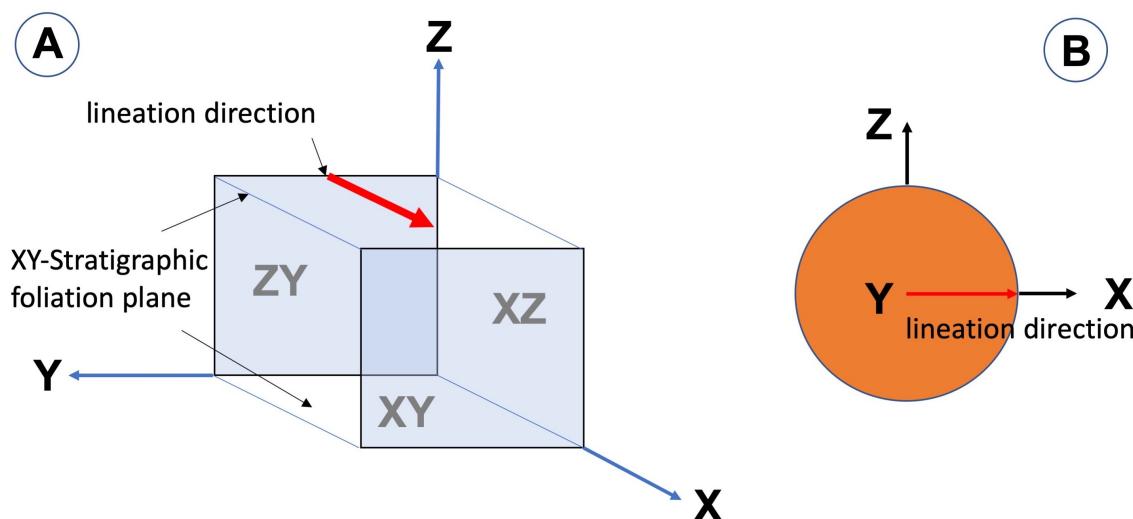
**Figure 3.** Sample Reference System and Pole figure representation. (**a**) Sample Reference System showing a simplified cubic sample with respect to the orthogonal reference. X, Y and Z axes are shown (**b**) Pole figure reference representation with X, Y and Z axes.

We used the non-disruptive method of the Quantitative Texture Analysis (QTA) by neutron diffraction. This method allows the evaluation of the Texture (also called Crystallographic Preferred Orientation, CPO) of the samples. It has been successfully applied to various types of rocks and synthetic materials: monomineralic quartzites [61], marbles [20], limestones [62], dunite [63] or glaucophanite [64], in poly-phasic rocks, as amphibolite [65,66], quartz-feldspatic mylonitic orthogneisses and gabbros [67,68], subacqueous lavas [69] or sandstones [70]. This procedure uses the high penetration and high flux of neutrons available at the nuclear reactor at the Institute Laue-Langevin (Grenoble, France) allowing the measurement of samples with volumes of approximately 1 cm$^3$ in one to eigth hours [71]. Here, we present the results from the D1B, D19 and D20 diffractometers (http://www.ill.eu). The raw data have been analyzed using the software package MAUD (Materials Analysis Using Diffraction [72]): diffracted intensities are used to calculate the Orientation Distribution Function (ODF [73]), from which the representative lattice planes are extracted and represented as Pole Figures (PF). PFs were represented showing the reference axes from the Sample Reference System (X, Y, Z in Figure 3). The coverage of the three-dimensional sample space has been acquired differently at the three beam lines (D1B, D19 and D19), due to their technical specifications. Briefly, D1B works at lambda=2.52Å, equipped with a position sensitive detector, covering a 2$\theta$ range of 128°; D19 is equipped with a very large (120°x30°) 2-dimensional position-sensitive detector, and works best in the wavelength range 0.8 to 2.4Å; D20 offers wavelength range 1.4 to 2.1Å and the position sensitive detector covers 153.6°. The respective angular settings are

167 reported in Table 2. The ODF was calculated using the E-WIMV approach [73]. The reliability of the
168 refinement is shown by the refinement parameters reported in Table 3. Calcite lattice parameters used for
169 the refinements are a=4.9849Å c=17.0479Å. 2Theta offset, sample position, and background parameters
170 were also refined.

**Table 2.** ILL instrument, setup and DOI. Acquisition time (sec) refers to a single phi-chi position

| Sample | Instrument | year | $\omega°$ | $\phi°$ | $\chi°$ | acquisition time (sec) | DOI http://doi.ill.fr/10.5291/ILL-DATA |
|--------|-----------|------|-----------|---------|---------|------------------------|----------------------------------------|
| 01BAS | D1B | 2016 | 10 | 0-355 | 0-90 | 20 | 1-02-201 [74] |
| 02SOD | D1B | 2016 | 10 | 0-355 | 0-90 | 20 | 1-02-201 [74] |
| 03SA1 | D19 | 2014 | 10 | 0-355 | 0-90 | 10 | 5-11-397 [75] |
| 04STE | D1B | 2016 | 10 | 0-355 | 0-90 | 20 | 1-02-163 [76] |
| 05CC2 | D1B | 2016 | 10 | 0-355 | 0-90 | 20 | 1-02-201 [74] |
| 06P1 | D1B | 2014 | 10 | 0-355 | 0-90 | 20 | 1-02-163 [76] |
| 08VP3 | D20 | 2005 | 10 | 0-355 | 0-90 | 40 | no DOI |
| 09MA1 | D20 | 2005 | 10 | 0-355 | 0-90 | 40 | no DOI |

**Table 3.** Quantitative Texture Refinement parameters

| Sample | Rb ref | Rexp ref | Rw ewimv | Rb ewimv | $F^2$ |
|--------|--------|----------|----------|----------|-------|
| 01BAS | 7.31 | 7.56 | 3.76 | 4.46 | 1.04 |
| 02SOD | 24.6 | 5.93 | 2.9 | 4.0 | 1.10 |
| 03SA1 | 27.19 | 25.62 | 24.11 | 24.43 | 1.732 |
| 04STE | 19.6 | 6.24 | 9.53 | 9.59 | 1.6 |
| 05CC | 9.22 | 3.96 | 4.11 | 4.57 | 1.26 |
| 06P1 | 15.79 | 6.28 | 4.85 | 5.95 | 1.005 |
| 08VP3 | 31.01 | 4.05 | 10.44 | 11.02 | 2.17 |
| 09MA1 | 22.83 | 4.98 | 12.91 | 15.73 | 1.18 |

171 The Seismic Properties were obtained using petrofabric data, as extensively explained by [7]. Here we
172 calculated the sample seismic properties by averaging the single crystal elastic tensor [77] weighted by the
173 ODF, as obtained by Quantitative Texture Analysis by neutron diffraction. In practice, the ODF calculated
174 using the Maud procedure was used to homogenize the single crystal tensor in Maud. Results for ODF
175 refinements are reported in Table 3. Although various averaging procedures can be adopted [78], we used
176 the arithmetic mean of Hill [79]. The resulting homogenized tensors were used in MTEX Matlab Toolbox
177 [80] to compute and plot seismic properties [81] shown in Figure 6. The same averaged tensors have been
178 then used to calculate the seismic anisotropies at different dip angles of the foliation plane, simply rotating
179 the tensors and changing the plane of projection for the pole figure in Figure 8. Pole figures in Figure 8 are
180 plotted in a way that only the Y axis remains constant and the observer is looking down from the Earth's
181 surface having the macroscopic foliation plane rotating with respect to the Y axis.

182 As a general consideration, this approach to computing seismic velocities generally produces higher
183 values when compared to natural samples. The most likely reason for this is that other important factors,
184 intrinsic and extrinsic, controlling seismic velocities and anisotropies are not included in the calculation.
185 These factors are fluid pressure, cracks density and their orientation, porosity, grain boundaries geometry
186 and their shape preferred orientation [5,53,82,83].

187 A thermodynamic approach [66,84] was also used to calculate the seismic properties of a modeled
188 carbonate rock at different pressure and temperature conditions, roughly corresponding to the estimate
189 conditions of texture development of the studied samples. We used the PerpleX software package (version

6.8.6 [85]) to compute the seismic parameters as dependent on the thermodynamic function G (molar Gibbs free energy), which is minimized to establish phases, amounts and compositions stable as a function of pressure and temperature. The software requires a chemical composition of the system as input. Software and data used for the calculation of phase relations and seismic velocities are freely available at http://www.perplex.ethz.ch. The graphical outputs were obtained using pyWerami source [86]. The calculated seismic properties correspond to those of a polycrystal rock with no preferred orientations. An averaged composition of carbonate rocks has been used as the model chemical system [87]. The model system composition (in wt %) is: $SiO_2$=3.02, $Al_2O_3$=0.56, FeO=0.39, MgO=0.75, CaO=52.40. In the computation $CO_2$ is considered saturated and, as solid solutions were chosen Do(HP) dolomite-ankerite solution, M(HP) for the magnesite-siderite solution, and Cpx(HP) clinopyroxene [88] and Perplex datafile repository. Holland and Powell (1998) [88] and successive update [89] (datafile hp62ver.dat at http://www.perplex.ethz.ch/datafiles/) was used as thermodynamic database. A typical output (Figure 7A) consists of pressure and temperature grid (in this calculation, P=1-15 kbar and T=100-1000°C) where the stable phases and assemblages are shown (i.e., pseudosection). Using the application Werami, which is part of the PerpleX package [85], specific properties were investigated in the P-T space and plotted in Figure 7B and 7C. Namely, we investigated the variations of modes, density, Vp and Vs of all phases within the investigated P-T ranges. Input data for PerpleX calculation may be found as supplementary materials.

**4. Results**

*4.1. Textures*

Figure 4 reports the calculated PFs for a single crystal-like of calcite, an aggregate of equigranular randomly-disposed crystals, and an aggregate of equigranular grains, by a statistical Fibre-Bingham distribution.
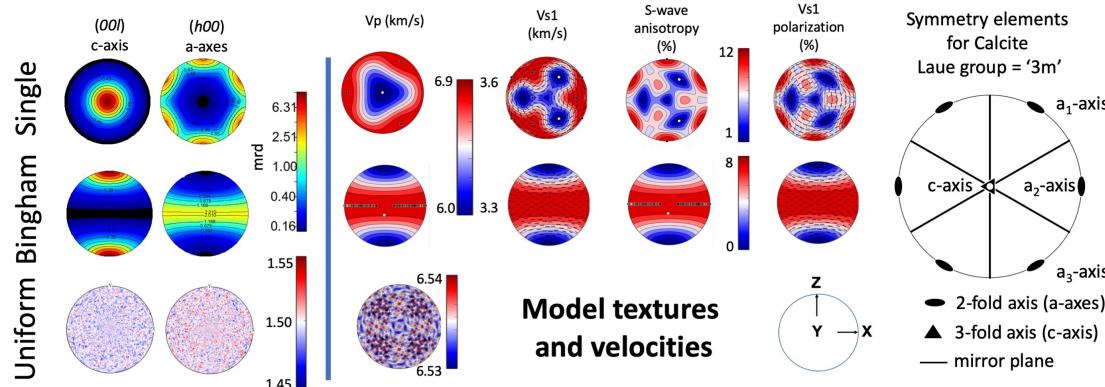
**Figure 4.** Pole Figures for model Textures and Seismic Velocities for Single Crystal-like, Uniform and Bingham Textured samples. Symmetry elements are shown for calcite crystal

They show the contributions to Texture expected by the crystallographic symmetry only or by textures: i) single crystal distribution is characterized by a strong c-axis maximum and a three-fold axes distribution in the plane normal to the c-axis; ii) oppositely, a random or uniform distribution of equigranular aggregate will reduce or obliterate the crystal symmetry anisotropy, producing a random statistical distribution, in any directions of the 3d space; iii) lastly, an imposed (e.g., tectonic stress) distribution, here represented as

217    the Fibre Bingham distribution [90], will produce strong maxima that follow neither the crystal symmetry
218    and nor a random distribution.

219       Figure 5 reports the pole figures representing the lattice planes (001), (110), (100) texture measured for
220    the studied samples. Calcite texture are commonly expressed showing c- and a-axes distributions (e.g. (001)
221    and (100)) and m-planes (110) since these orientations better describe the deformation mechanisms active
222    during plastic deformation at lattice scale and are commonly reported in the literature. Table 3 reports
223    the R factors and $F^2$ factor, commonly used in texture analysis to assess the quality of ODF refinement.
224    In general, the samples show different texture distributions and densities but they can be divided into 2
225    principal types: a random distribution (01BAS, 06P1); c-axis textured distribution (02SOD, 03SA1, 04STE,
226    05CC2, 08VP, 09MA). The c-axis textured distribution may be further divided into orthorhombic (02SOD,
227    05CC2, 09MA) and monoclinic symmetry (03SA1, 04STE, 05VP) types. The orthorhombic type (A) is
228    characterized by parallelism between the (001) poles and the Z direction. On the other hand, monoclinic
229    type (B) shows an angle between the (001) poles cluster and the Z direction. Symmetrically, the (100) poles,
230    which generally display a girdle distribution, may lay orthogonal to the Z direction or with an angle,
231    generally 30 to 45 degrees. $F^2$ values (Table 3) may be used as overall index to assess the randomness of
232    the texture [91,92]. As expected for poorly textured samples, 01BAS, 06P1 have $F^2$ close to 1 $mrd^2$, even
233    though 01BAS displays a minimum amount of preferred orientation. 02SOD, 04STE, 05CC2 and 09MA are
234    characterized by well developed textures, though the $F^2$ index is relatively low, being between 1.10 and
235    1.26 $mrd^2$. Higher $F^2$ values are shown by 03SA1 and 09MA.
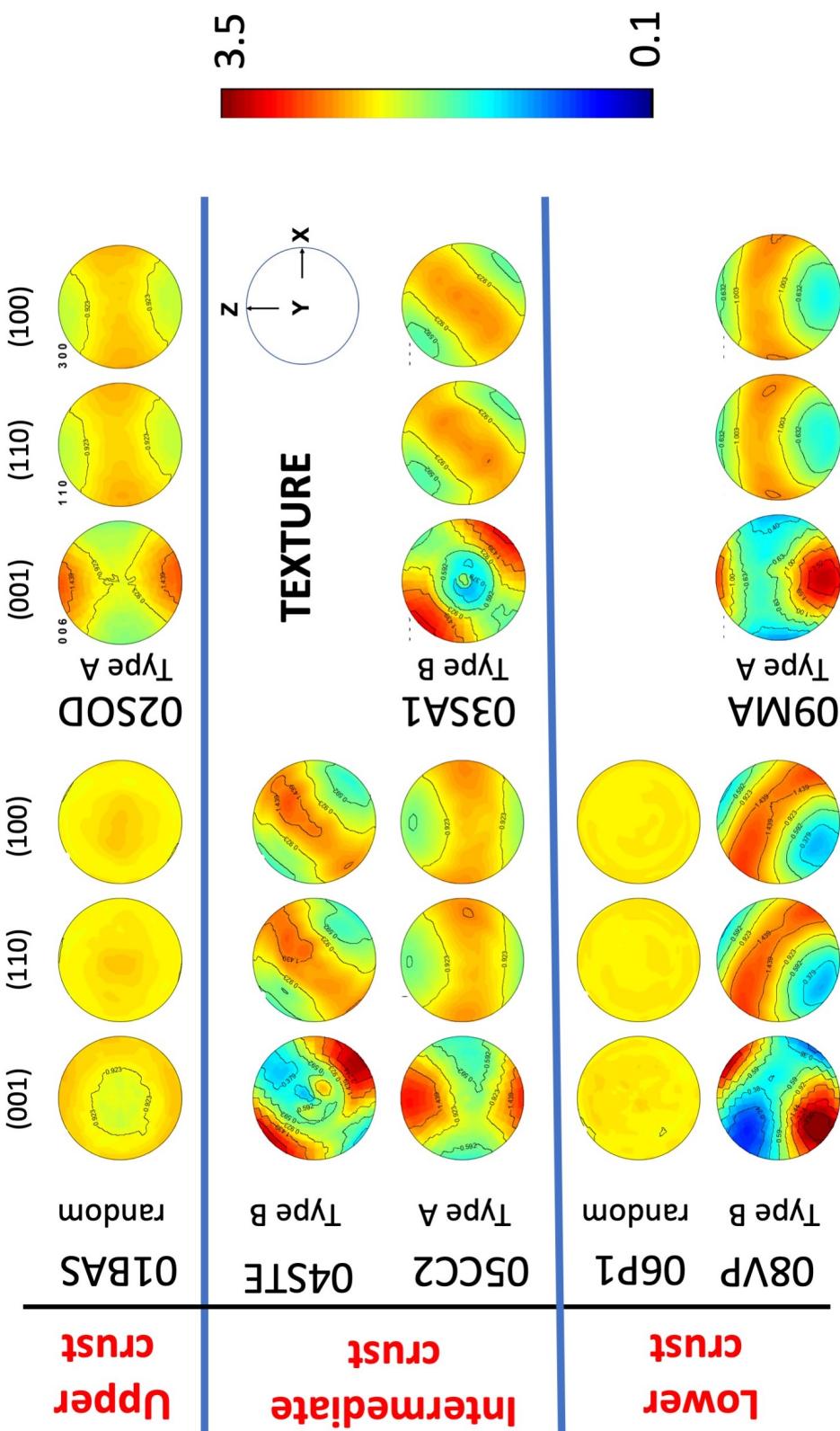
**Figure 5.** Texture for the studied sample. Pole Figures represents density contours of poles to plane (001), (110), (100), in multiple of uniform distribution (mud). Axes reference as in Figure 3b

*4.2. Seismic Velocities*

Figure 6 reports the calculated seismic velocities. Namely, P-wave Vp (km/s), S-wave anisotropy and Vs1 and V2 polarization. Their distributions closely resemble the main texture feature (Figure 5). In fact, since the c-axis direction is the slowest Vp in the single crystal setting, and the a-axes directions are close to fastest (Figure 3), the general feature that shows up is that the pole to (001) distribution correspond to the slowest directions in the Vp plots. So, the prediction of the slowest direction in carbonate rocks is relatively straightforward since it is influenced by the c-axis distribution. In contrast, S-wave anisotropies are more complex to predict since they result from a combination of textures (Figure 5). Specifically, 02SOD, 06P1, 08VP and 09MA display a girdle distribution of the poles to (100) and (110), which correspond to a pronounced direction of fastest propagation. Conversely, 01BAS, 03SA1 and 05CC2 are characterized by single or multiple clusters for S-wave anisotropies, giving a more complex pattern of polarization. 04STE displays a mixed distribution, where a weak fastest S-wave girdle links the two clusters.
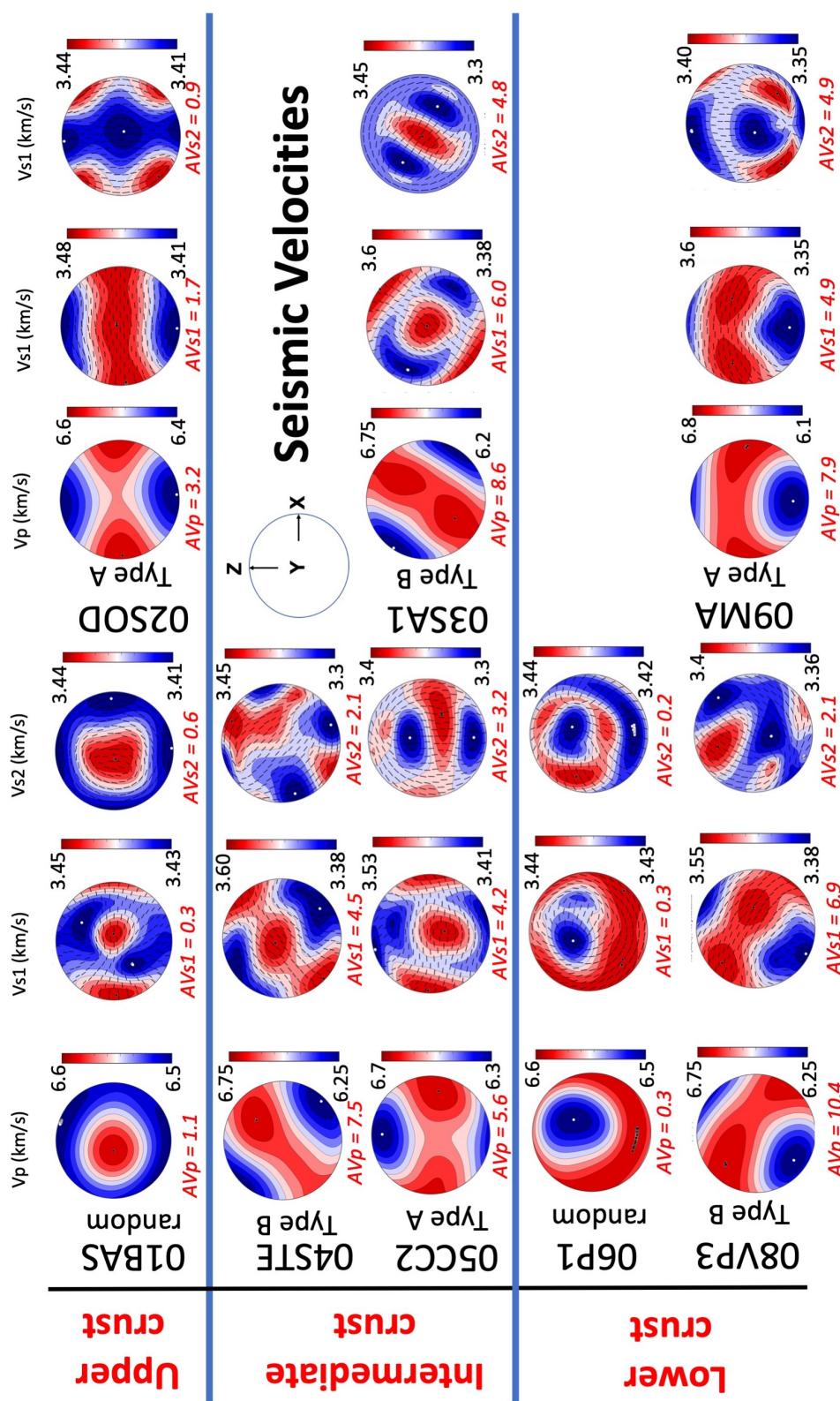
**Figure 6.** Vp(km/s), Vs1 (km/s) and Vs2 (km/s) seismic waves velocities for the studied samples. Anisotropy for Vp (AVp), Vs1 (AVs1), Vs2 (AVs2) are calculated as A = 200*(maxV-mivV)/(maxV+minV). For AVp V=Vp, for AVs1 V=Vs1, for AVs2 V=Vs2.

**Table 4.** Homogenized Elastic Tensors for the studied samples - [GPa] - density = 2.712 g/cm3

**Single Crystal**

| 124.80639 | 54.72449 | 51.150898 | 0 | -3.4680943 | 0 |
|---|---|---|---|---|---|
| - | 124.80639 | 51.150898 | 0 | 3.4680943 | 0 |
| - | - | 100.81746 | 0 | 0 | 0 |
| - | - | - | 30.698822 | 0 | 3.4680943 |
| - | - | - | - | 30.698822 | 0 |
| - | - | - | - | - | 35.04095 |

**Model Bingham**

| 127.50047 | 51.043633 | 55.929905 | 0 | 0 | 0 |
|---|---|---|---|---|---|
| - | 96.653496 | 51.04301 | 0 | 0 | 0 |
| - | - | 127.4964 | 0 | 0 | 0 |
| - | - | - | 30.140978 | 0 | 0 |
| - | - | - | - | 35.78422 | 0 |
| - | - | - | - | - | 30.141603 |

**01BAS**

| 115.48373 | 51.741405 | 52.193005 | 0.0137869865 | -0.15203768 | -0.057538427 |
|---|---|---|---|---|---|
| - | 115.00182 | 52.065735 | -0.015753072 | -0.070318885 | -0.06224491 |
| - | - | 117.33802 | 0.003552162 | -0.22920334 | 0.008067851 |
| - | - | - | 32.058846 | 0.005816382 | -0.07812717 |
| - | - | - | - | 32.197884 | 0.013756884 |
| - | - | - | - | - | 31.695593 |

**02SOD**

| 119.29561 | 51.75047 | 52.70474 | 0.09108701 | -0.13749328 | 0.24086875 |
|---|---|---|---|---|---|
| - | 112.01606 | 51.493103 | 0.1646471 | -0.030619144 | 0.2721084 |
| - | - | 116.93503 | 0.13448612 | -0.15284155 | 0.118958846 |
| - | - | - | 31.385612 | 0.13175486 | -0.03567471 |
| - | - | - | - | 32.75555 | 0.09919309 |
| - | - | - | - | - | 31.68194 |

**03SA1**

| 108.98519 | 51.129845 | 53.54879 | -0.22707361 | 0.09098859 | 4.010708 |
|---|---|---|---|---|---|
| - | 115.68208 | 54.011932 | -0.42028734 | 0.19944625 | 4.040168 |
| - | - | 120.24887 | -0.4792106 | 0.6209795 | 1.0868437 |
| - | - | - | 34.00615 | 1.3028204 | 0.21294828 |
| - | - | - | - | 33.391453 | -0.24855585 |
| - | - | - | - | - | 30.711746 |

**04STE**

| 114.62599 | 51.28098 | 52.65128 | 0.40403882 | -0.24915834 | 4.076245 |
|---|---|---|---|---|---|
| - | 113.24674 | 52.87957 | 1.7690595 | 0.1510593 | 2.9629822 |
| - | - | 120.20226 | 1.3745261 | -0.33024174 | 1.3390523 |
| - | - | - | 32.772617 | 1.5227332 | 0.12351844 |
| - | - | - | - | 32.543037 | 0.45559624 |
| - | - | - | - | - | 31.0105 |

**05CC2**

| | | | | | |
|---|---|---|---|---|---|
| 120.331055 | 52.018433 | 53.357944 | -0.5572579 | 0.46192774 | -0.14939365 |
| - | 109.84183 | 51.32877 | -2.052971 | 0.22327025 | -0.38076687 |
| - | - | 117.142975 | -0.3637613 | 0.20798893 | 0.034985803 |
| - | - | - | 31.15168 | 0.02339253 | 0.23576291 |
| - | - | - | - | 33.43074 | -0.6357612 |
| - | - | - | - | - | 31.877514 |

**06P1**

| | | | | | |
|---|---|---|---|---|---|
| 116.18255 | 52.0272 | 51.979866 | -0.04868714 | -0.03236508 | -0.011777747 |
| - | 116.03572 | 51.9618 | -0.16846395 | -0.021853263 | -0.021358635 |
| - | 51.9618 | 115.6278 | -0.067962535 | -0.08895395 | -0.020873472 |
| - | - | - | 31.94424 | -0.021930851 | -0.02458574 |
| - | - | - | - | 31.965382 | -0.053988267 |
| - | - | - | - | - | 32.021183 |

**07P2**

| | | | | | |
|---|---|---|---|---|---|
| 117.62099 | 51.808167 | 52.04327 | 0.26321256 | 0.320841 | 0.538134 |
| - | 115.71749 | 51.596924 | 0.7797489 | 0.24568443 | 0.40074456 |
| - | - | 115.65552 | 0.5507176 | 0.31947044 | 0.02256278 |
| - | - | - | 31.551678 | 0.03927036 | 0.26017663 |
| - | - | - | - | 32.037464 | 0.29400057 |
| - | - | - | - | - | 31.800737 |

**08VP3**

| | | | | | |
|---|---|---|---|---|---|
| 117.58365 | 52.024033 | 53.17902 | 0.9461038 | 1.649634 | -5.2456484 |
| - | 111.576004 | 52.19252 | 3.4886246 | 0.64441526 | -4.231288 |
| - | - | 119.872314 | 3.4239075 | 1.0557145 | -1.510464 |
| - | - | - | 31.833376 | -1.7366006 | 0.750887 |
| - | - | - | - | 32.96562 | 1.1209756 |
| - | - | - | - | - | 31.585485 |

**09MA1**

| | | | | | |
|---|---|---|---|---|---|
| 123.13773 | 51.935154 | 53.12128 | 1.066385 | 0.72052747 | -0.34793347 |
| - | 108.63644 | 51.16951 | 3.118211 | 0.10843302 | -0.30422294 |
| - | - | 117.85145 | 3.0853832 | 0.26028427 | 0.001484112 |
| - | - | - | 30.831026 | -0.014819718 | 0.1207543 |
| - | - | - | - | 33.11233 | 1.2279662 |
| - | - | - | - | - | 31.690102 |

## 5. Discussion

### 5.1. Texture types evolution with temperature, pressure, shear geometry and strain

Texture data reported in Figure 5 fall into the types of calcite texture most commonly described for natural rocks [93] and reported in experimental results [16,17,94,95]. In particular, we separated two types: random, where no or a little preferred orientation is found, and textured, characterized by a strong c-axis maximum and a-axes girdle distribution. Textured types have been further separated in Type A and Type B, to emphasize the relations between Texture and shear plane, as described for pure shear (i.e., orthorhombic geometry, Type A) and simple shear (i.e. monoclinic geometry, Type B) [20,93,96]. Type A and B have been used to infer the deformation regime and the sense of shear (e.g. [97–100]). However, Pieri et al. (2001)

257  [101] demonstrated the risk of simplifying those textural relations with deformational regimes. In fact, the
258  most common calcite deformation mechanisms may allow, even at low temperature, a quick transition
259  from monoclinic to orthorhombic symmetries, even under a simple shear regime and at low strain (>2).
260  Similar observations have been made on naturally deformed marbles [102]. Accordingly, the studied
261  samples also show that discriminating between high temperature (HT) and low temperature (LT) textures
262  is not an easy task. For example, 02SOD, 05CC2 and 09MA1 samples, though their textures developed
263  respectively at ≈200°C, 300-350°C, and 600-750°C (Table 1), they all display a similar orthorhombic
264  symmetry; specularly, 04STE, 03SA1, 08VP share the same texture but developed at different temperatures,
265  300-350°C, ≈350°C, and 700-800°C (Table 1). Literature data, between **100 and 400°C** at increasing shear
266  strain, suggest a general evolution from Type A texture, generally far from the shear zone core, to Type
267  B textures and, more often, the coexistence of Type A and B [82]. Type A seems to become dominant at
268  very high shear strain values and very high pressures [16,103]. At low temperature (<300°C) and low
269  pressure (<3kbar), as in carbonate fault gouges or thrust systems, Type B is generally favorite [104–106]
270  while A and B types start to compete where temperature, pressure and shear strain all overcome certain
271  thresholds. These threshold values are hard to quantify; most likely pressure should exceed 3-4 kbar
272  and shear strain 1-2 [13,16,82,96,103,106]. Similar competing textures were also described for dolomite
273  deforming between 240-300°C under simple shear geometry [107]. Besides, the recent experimental work
274  of Schuster et al. (2019) [16] shows that very high shear strains (>80) tent to stabilize Type A texture that
275  replaces early A or B types. This experimental work also strongly supports the findings by Ebert et al
276  (2007) [103] that constrained similar evolution from field observations. In particular, Ebert et al (2007) [103]
277  showed evolving random to Type A and B textures as temperature and shear strain increase. Ebert et al
278  (2007) [103] also showed textures similar to those of 04STE and 03SA1 samples where the angle between
279  the c-axis maximum and the Z axis is much higher than typically described.

280      Similar considerations may be done on metamorphic marbles produced at intermediate temperature
281  (≈400-600°C) and pressures related to subduction-collisional tectonics (≈10-20 kbar). In particular, the
282  large literature available on the Carrara Marble allow us to constrain textural types with shear strain
283  geometry and grainsize. Large (1-2 mm) to intermediate (0.1-0.5mm) grainsize marbles, characterized
284  by granoblastic textures may show random texture [53,108] as well as Type A [52]. The first most likely
285  due to static annealing or larger scale strain-partitioning and the second associated with grain boundaries
286  migration and subgrain rotation dynamic recrystallization processes [32]. In marbles showing shape
287  preferred orientations and microscopic foliation, the Type A is better developed [20] suggesting a high
288  shear strain condition. Experimental work on Carrara marbles under torsion [109], ranging between 500
289  and 700 °C and shear strain from 0 up to 50, support the observations [110] that Type A easily stabilizes
290  at high strain conditions replacing Type B, no matter if coaxial and non-coaxial. Again, this process
291  seems to be more likely occurring at high temperatures (>500°C) [110]. Barnhoorn et al. (2004) [109]
292  also showed that at low temperature (≈500°C) random texture may replace Type B textures increasing
293  shear strain. Other intermediate temperature marbles (400-500°C), from elsewhere (e.g. [11,102,111,112])
294  support this shift from B to A types texture. However, no shear strain constraints are available to include
295  these observations in the above scheme. Higher temperature (>600°C) marbles, similar to samples 08VP3
296  and 09MA1, naturally [22] or experimentally [14,109] deformed do not show a strong shift from B to A
297  type texture. These observations may be taken to support the idea that shear strain most likely controls the
298  textural type, more than temperature. However, more observations are needed to build a valid general
299  scheme. More observations are also needed to produce a solid scheme to relate deformation mechanisms
300  with the observed textures. The texture observed in these samples do not uniquely relate to specific
301  deformation mechanisms. Type A and B textures are present in samples where intra-crystalline slip
302  mechanisms are relevant, as 08VP3 and 09MA1. On the other hand, where twinning is present, together
303  with grainsize reduction deformation mechanism (02SOD, 04STE, 05CC2), both Type A and Type B may

304   develop [100]. Moreover, the combination of sub-grain rotation mechanisms, known to be important at
305   similar conditions [16], and grain-boundary migration may have contributed to the observed random
306   texture in P1.

307   *5.2. Seismic anisotropy*

308       Seismic velocities and anisotropy of carbonate rocks in the studied samples change with texture types
309   (Figure 6). Vp velocities vary from a minimum of 6.1 km/s to a maximum of 6.8 km/s; AVp anisotropy
310   varies between 0.3 and 10.4 (Figure 6).  Vs varies from 3.3 and 3.6 km/s, while Vs1 anisotropy varies
311   between 0.3 and 6.8.  The direction of maximum Vp varies from parallel to X direction of the fabrics
312   (05CC2, 02SOD, 09MA), corresponding to Type A texture, to more than 45 degrees in the XZ plane (04STE,
313   03SA1, 06P1, 08VP3), for Type B texture. Vp displays a general girdle distribution that roughly describes a
314   plane of max Vp. Max Vp plane changes its orientation even within the same group of Vp max direction.
315   Vp max in Type B samples has an angle with X direction that varies between 20 to 50 degrees.  More
316   interestingly, the Vp maximum frequently dips about 20-30 degrees away from the circumference (XZ
317   plane). Similarly, the Vp max girdle plane dips between 20 to 50 degrees from the plane of shear.  Besides,
318   Vs velocities frequently show a double to triple maxima distributions.  A large literature is available
319   for sedimentary rocks, though the large majority is dedicated to shales and sandstones (see complete
320   review [7]). Similar Vp and Vs values have been measured and calculated for calcite [13,22,82,113,114]
321   at different temperature and depth conditions. Vp velocities most frequently show a girdle distribution
322   of maxima variably dipping to the plane of shear, recalling Type A and Type B distributions. In general,
323   the Vp and Vs velocities overlap with those calculated for our samples, a part for those samples from
324   very shallow depth (<1000m) [113,114] where only after reducing porosity and increasing cementation the
325   Vp values go from low (<5km/s) to higher values, more similar to those here measured and calculated
326   (>6 km/s). These observations support the general idea that carbonate rocks anisotropy also contributes
327   to the overall anisotropy of the crust [7,22,82], at any depths.  To further investigate the nature of this
328   anisotropies we calculate the seismic isotropic component by the thermodynamic modeling described in
329   chapter 3. The thermodynamic modeled seismic velocities, Vp and Vs (Figure 7), describe a range of Vp
330   wave velocities from ≈ 6.0 km/s to 6.5 km/s. Vs velocities vary from 2.6 to 3.0 km/s. The P-T plots in
331   Figures 7B and 7C are characterized by three main parts where Vp and Vs vary progressively as a function
332   of the changing mineral assemblages and mode proportion, as described in the pseudosection of Figure
333   7A. The three sectors are characterized by: i) the presence of aragonite instead of calcite a high pressure
334   and low temperature; ii) the association of calcite and dolomite at intermediate temperature and pressure
335   from low to high; ii) the stabilization of clinopyroxene at high temperature, for low to high pressures. In
336   general, Vp and Vs wave velocities decrease moving toward higher temperatures and increase moving
337   toward higher pressures. According to the pressure and temperature constraints for the studied samples
338   (Table 1) we are below the aragonite phase transition and the Vp should vary from 6.0 to 6.5 km/s, and Vs
339   from 2.8 to 3.0 km/s. The calculated values from texture analysis [68,84] as well as those reported in the
340   literature, differ by about 10% from these calculated values. These values are generally closer to measured
341   seismic velocities taken orthogonal to the maximum shear direction (i.e., lineation) [53] or in the more
342   isotropic samples or very shallow sample, dominated by low porosity (<10%) [114]. Consequently, these
343   Vp and Vs can be used as a reference for the isotropic component of carbonate rocks, to investigate the
344   amount of anisotropy to be expected when observing real seismic data for similar rock composition. In
345   general, the analyzed samples show an increase of seismic velocities due only to textural anisotropies
346   that can be about 0.2 to 0.8 km/s for Vp and 0.3 to 0.6 Vs.  These results show that seismic properties
347   (e.g., velocities and anisotropies) even for a single rock type (e.g., carbonate rocks) may strongly change in
348   the crust, as function of temperature, pressure, and shear strain, as a result of texture types that strongly

349 control seismic propagation. Similar considerations have been proposed for other rock compositions. In
350 these rock types specific mineral phases showed preferred orientations that produced relevant deviations
351 from the isotropic component of the seismic properties (e.g. [7,13,23,84]). This evidence suggests that at
352 depth there is important overlapping between different rock types in term of their seismic properties, such
353 that unambiguous determination of geological information from natural seismic data imply a combined
354 use of many parameters [115]. In addition, it is clear that also the orientation of the macroscopic fabric,
355 shear foliation, lineation, or any fabric associated with texture in rock-forming minerals play an important
356 role in defining seismic anisotropies [24,84].
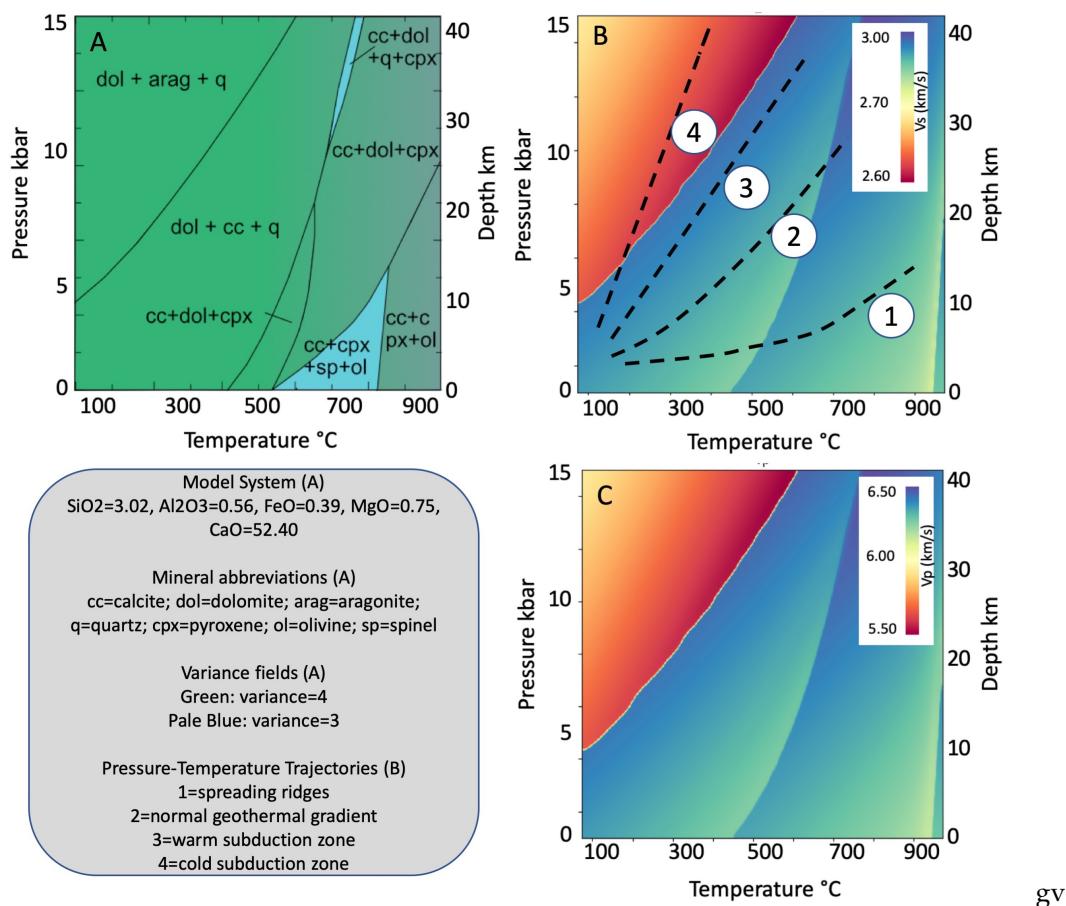
**Figure 7.** A) Pseudosection calculated using Perple_X thermodynamic packages [85]. B) Vs (km/s) seismic waves contour diagram. C) Vp (km/s) seismic waves contour diagram. Geothermal gradients in B after Cloos (1993) [116].

357     To further investigate the relevance of the orientation of the shear plane at different depth in the crust,
358 we used the approach of Ko and Jung (2015) [24] by rotating the shear flow plane around the Y axis. In
359 Figure 8 the results are shown by changing the plane of view, from XZ, used in Figures 3, 4, 5, 6, to XY.
360 Figure 8 shows the progressive variations of the seismic properties by changing the dip angle from 0 to
361 90 degrees (0, 30, 45, 70, and 90). From the resulting rotated tensors, the components of Vp, Vs1 and Vs2
362 were read parallel to the horizontal component of the X direction (X' in Figure 8), as well as parallel to the
363 normal to the Earth's surface (T in Figure 8). Random textures are characterized by a constant Vp and
364 Vs2 maxima parallel to the Y direction and the lowest direction being within the X'T plane. The lowest
365 velocity is always recorded parallel to the vertical T direction, at any dip. A relevant deviation is found

366   for the Vs1 where the highest velocities parallel to T are recorded at dip >45 degrees, while parallel X'
367   at dip <45. Type A shows relatively similar features for samples at different depth, with a general trend
368   with the X' component of Vp which decreases for steep dipping shear zones, while the T component
369   increases, becoming the fastest at depth >30-45 degrees. The Vs1 component generally decreases for the
370   three samples at different depth, but it is steeper for the lower crust sample (e.g., 08MA1). On the other
371   hand, Vs2 components show that the intermediate crust sample 05CC2 has a different trend compared to
372   the other samples. Type B has more diversification than Type A, Vp parallel to T may vary from slowest to
373   fastest, independently by the dip. 08VP3 and 06P1 show the fastest values parallel to T at dip>30. Vs1 and
374   Vs2 fastest are more commonly found at Y for 03SA1 and 04STE intermediate crust samples, while in 06P1
375   Vs1 fastest velocities describe a girdle close to the X'T plane at any dip and in 08VP3 sample become closer
376   to T at dip>45. Vs2 velocities Vs2 fastest velocities are in the direction of Y for 03SA1 at any dip while
377   they are highly variable for the sample 04STE. Girdles with maxima characterize Vs2 in 06P1 and 08VP3,
378   producing highly heterogeneous distribution at different dip.
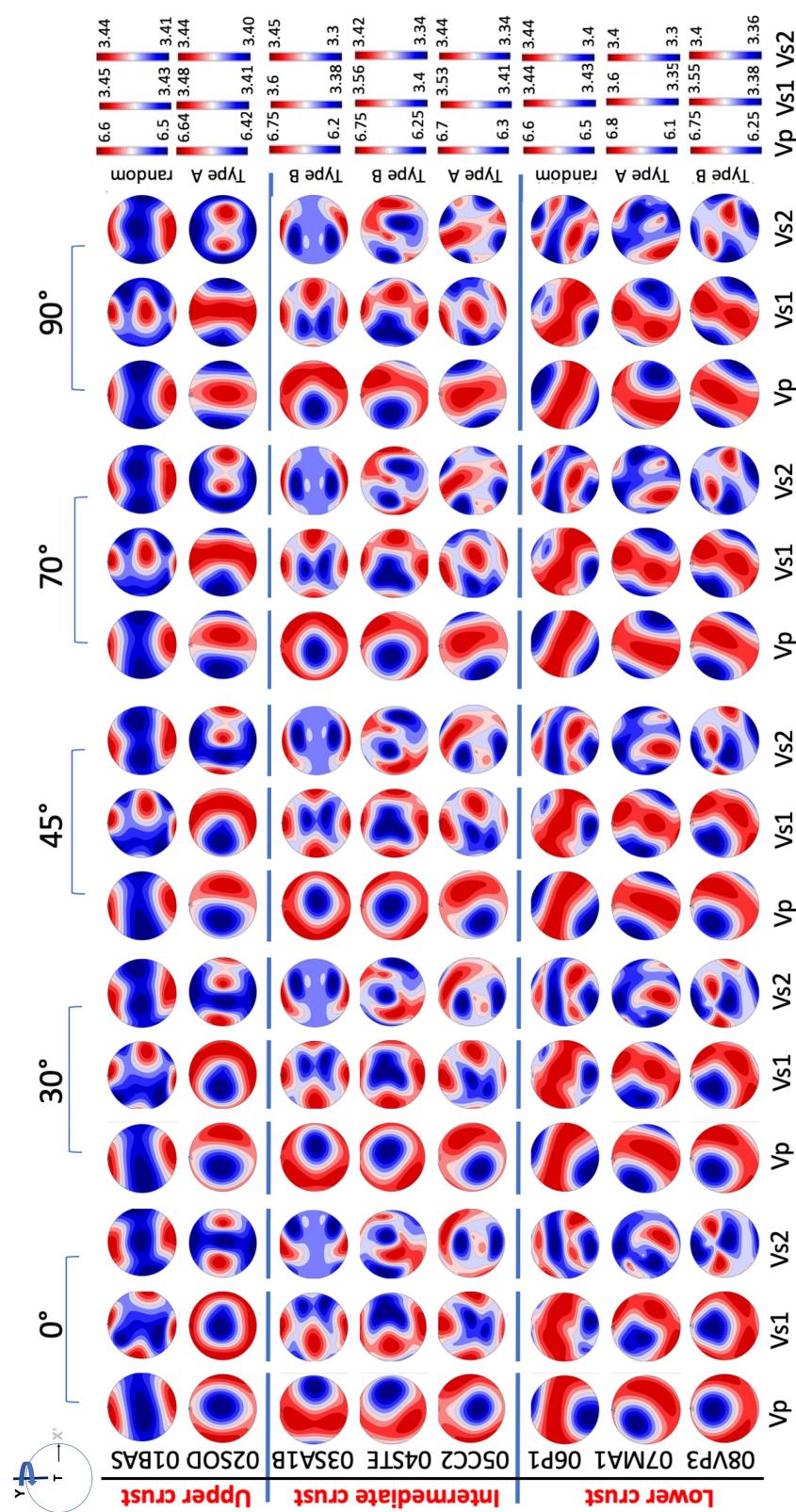
**Figure 8.** Pole Figures representing the P- and S- (S1 and S2) seismic velocities for calcite at different depth and dipping angle of the main macroscopic fabric plane (e.g. shear plane or stratification). X′ correspond to the horizontal component of the X fabric axis while T correspond to the normal to the horizontal surface.
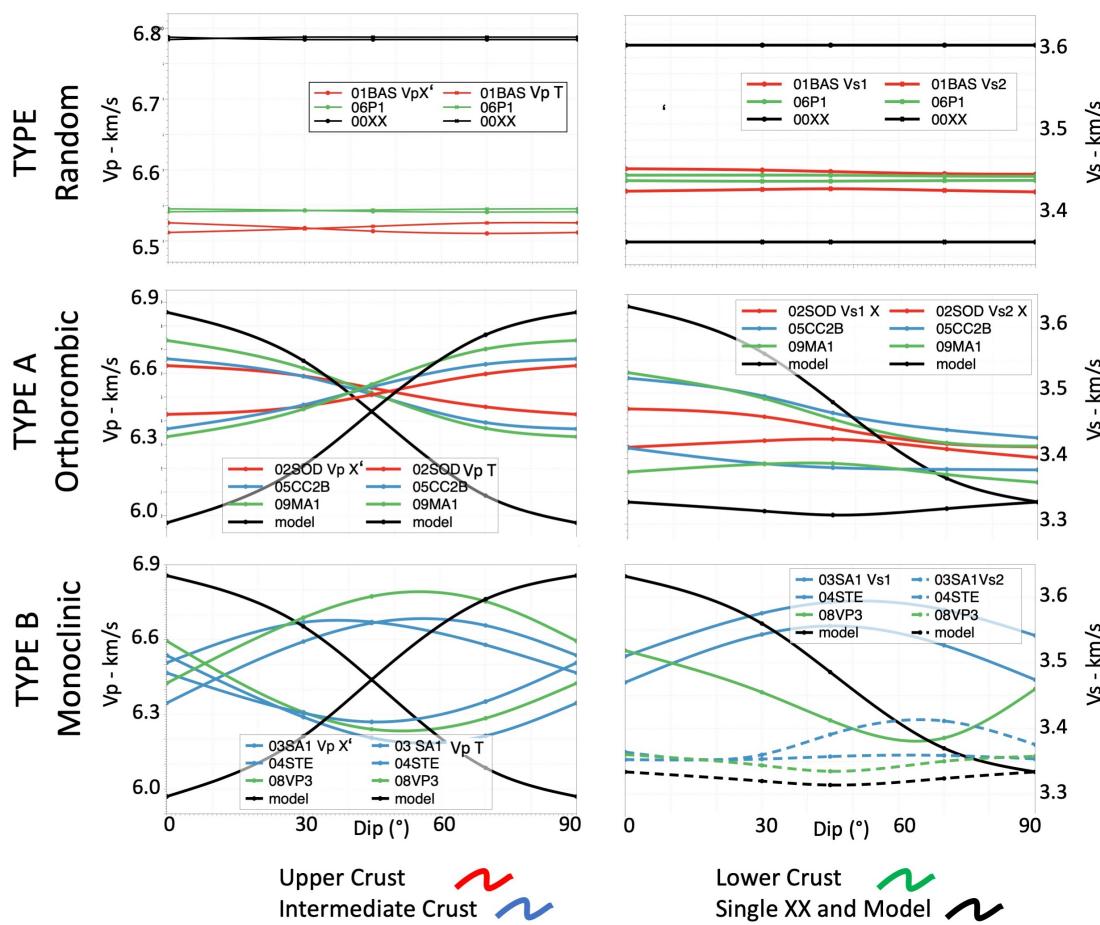
**Figure 9.** Vp components propagating horizontally (X' component) and vertically (T component) - Vs1 and Vs2 horizontal component (of X)X'). See text for explanation

In the Type B distribution, the lower crust sample 09VP3 displays an opposite trend to the intermediate crust samples 03SA1 and 04STE. In particular, while for the intermediate crust samples the horizontal Vp and Vs1 values increase from 0 to 45-50 degrees and then decrease approaching vertical dipping, the lower crustal sample 08VP3 starts decreasing and then, at about 60 degrees dip, increases. These heterogeneities also occur for vertical Vp and Vs2 components. The Vp vertical component closely mirrors the Vp horizontal, while the Vs2 components are less sensitive to the dip variation, being in a smaller interval, generally < 0.1 km/s.
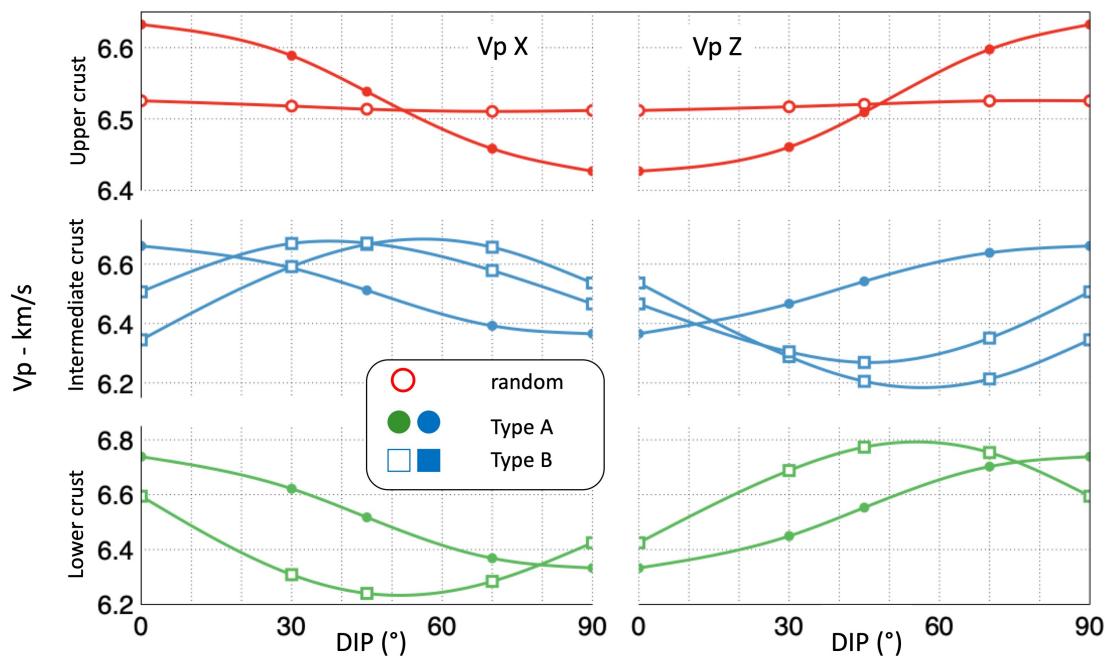
**Figure 10.** Vp crustal section. upper crust = red, intermediate crust = blue, lower crust = green. Texture types: A = hollow circle; A = full circle; B = hollow square

Figure 10 represents the Vp velocities at different depths, at varying dip. From 0 to 15 degrees dipping of the shear planes, as those generally developed along the flat part of thrust systems [9], the Type A textures produce higher Vp velocities propagating horizontally, parallel to X' component (Figure 8) and slower parallel to the normal to the topographic surface (T component in Figure 8). This setting does not change with depth, while the fastest Vp velocities are recorded at depth (i.e., lower crust). This pattern is reversed at different dip angles: upper crust at 50 degrees, intermediate crust between 20 and 30 degrees, and the lower crust at 80 degrees. At intermediate crust conditions, this flip may correspond to the evolution of the thrust system from flats to ramps. The change of dip correspond to a substantial increase of Vp velocities parallel to X', from 6.4 to 6.7 km/s. At the same depths, it corresponds a decrease parallel to T for rocks having a Type B texture pattern. Oppositely, at depth, both Type A and B produce an overall decrease of horizontally propagating velocities, from 6.8 to 6.3 km/s and from 6.6 to 6.2 km/s, respectively. Type B reaches its minimum at 50 degrees and then increases slowly approaching vertical dips. In general, steep dipping shear zones, as those in transtensional or transpressional systems (e.g., positive and negative flower structures), will produce slower or at maximum equal Vp velocities propagating horizontally (X') than shear zone within the same system but with lower dipping angles (Figure 10). Figure 11 represents the evolution of Vp seismic velocities (vertical component T) with depth at changing dip angles. Figure 11 also reports the predicted P-wave velocities in the continental crust as modeled by Lloyd et al. (2011) [23] for 'rock recipes'. Vertical red boxes correspond to Vp ranges for middle to lower crust proposed by Rudnick & Fountain (1995)[117]. Two aspects arise from this image. Firstly, carbonate rock may overlap with average rock types or 'recipes' at various depth in the continental crust. Large discrepancies to these overlapping may arise by the dipping of the shear planes. At similar depths, Vp velocities may differ of about 0.3-0.5 km/s, only due to different dipping. Secondly, a specific patter is reproduced by Type A texture, at any depth. Type A texture shows is characterized by an increase of Vp velocities as the dipping angle increases. This pattern is reproduced at the three different depths our samples represent. Moreover, Types B displays more variability in the way seismic velocities change with dipping of the shear plane.
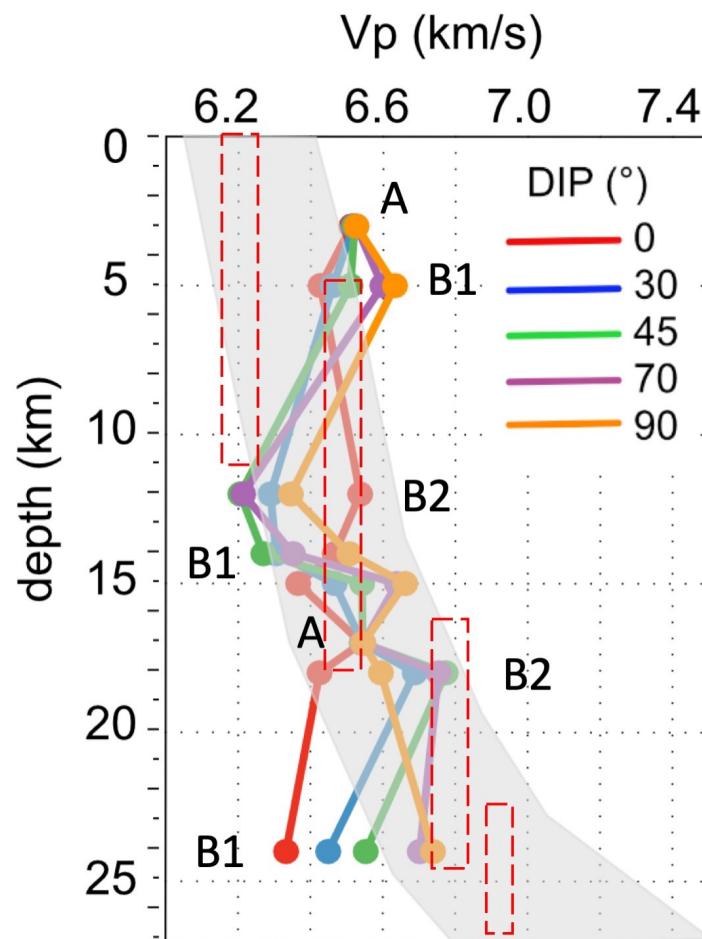
**Figure 11.** P-wave velocity propagating vertically (T component of Figure 8) crustal profile based on the data presented in this work for carbonate rocks at different depth and dip angle of the shear plane. Grey are correspond to the predicted P-wave velocities in the continental crust as modeled by Lloyd et al. (2011) [23]. Vertical red boxes correspond to Vp ranges for middle to lower crust Rudnick & Fountain (1995)[117]. A, A, and B texture Types described in the text.

## 6. Conclusions

- Eight samples of limestones and marbles were studied by neutron diffraction. We collected Texture of naturally deformed calcite at different depths in the crust, from upper to lower crust.
- Different Texture patterns were recognized, from random to strongly textured (Type B); the latter, with orthorhombic (Type A) or monoclinic (Type B) symmetries. Seismic anisotropies were calculated using the Orientation Distribution Function to homogenize the elastic tensor of calcite.
- A wide variability of seismic anisotropies arise from the various textural types, crustal positions and dipping of the shear planes.
- These results may be valuably used to guess geometry of shear zones at upper to depth for carbonate rocks or at deeper crustal levels where thick carbonatic horizons are involved localizing deformation (Figure 11).
- This work suggests that at depth, even for carbonate rocks, there is an important overlapping between different rock types in term of their seismic properties (Figure 11); unambiguous determination of geological information from natural seismic must consider the orientation of the macroscopic fabric,

425     shear foliation, lineation, or any fabric associated with texture playing a role in developing seismic
426     anisotropies [24,84].
427     ● More work still needs to be done to include other parameters influencing seismic anisotropies,
428     intrinsic and extrinsic, to build a database of natural rocks properties [5–7,13,23].
429     ● Lastly, texture types may produce unique seismic velocities pattern. For example, Type A (Figure 11)
430     produce a unique pattern at any depth, characterized by an increase of Vp velocities (e.g., 6.3 to 6.8
431     at 20-25km depth) as the dipping angle increases. Future studies may show if these singular pattern
432     might be used to better constrain the interpretation of seismic profiles.

433 **Author Contributions:** All authors participated in the preparation of this manuscript. M.Z. conducted sample
434 collection, collaborated neutron experiments, data analysis and prepared the first version of the manuscript. D.C.
435 worked on neutron experiments and data analysis. B.O. worked on neutron experiments and data analysis

436 **Funding:** Neutron experiments were funded by ILL (www.ill.eu)

437 **Acknowledgments:** Two anonymous reviewers are greatly thanked for their help to produce the present form

438 **Conflicts of Interest:** The authors declare no conflict of interest.

## References

440 1.     Lowrie, W. *Fundamentals of Geophysics*; 2007. doi:10.1017/cbo9780511807107.
441 2.     Sun, L.; Fang, C.; Sa, L.; Yang, P.; Sun, Z. Innovation and prospect of geophysical technology in the
442     exploration of deep oil and gas. *Shiyou Kantan Yu Kaifa/Petroleum Exploration and Development* **2015**, *42*, 414–424.
443     doi:10.1016/S1876-3804(15)30038-0.
444 3.     Kendair, J.M.; Maddock, J.; Hall, S.A.; Fisher, Q.J. Seismic anisotropy as an indicator of reservoir quality in
445     siliciclastic rocks. *69th European Association of Geoscientists and Engineers Conference and Exhibition 2007: Securing*
446     *The Future. Incorporating SPE EUROPEC 2007* **2007**, *5*, 2614–2618. doi:10.1144/SP292.7.
447 4.     Okaya, D.; Vel, S.S.; Song, W.J.; Johnson, S.E. Modification of crustal seismic anisotropy by geological structures
448     ("structural geometric anisotropy"). *Geosphere* **2019**, *15*, 146–170. doi:10.1130/GES01655.1.
449 5.     Faccenda, M.; Ferreira, A.M.; Tisato, N.; Lithgow-Bertelloni, C.; Stixrude, L.; Pennacchioni, G. Extrinsic Elastic
450     Anisotropy in a Compositionally Heterogeneous Earth's Mantle. *Journal of Geophysical Research: Solid Earth*
451     **2019**, *124*, 1671–1687. doi:10.1029/2018JB016482.
452 6.     Brownlee, S.J.; Schulte-Pelkum, V.; Raju, A.; Mahan, K.; Condit, C.; Orlandini, O.F. Characteristics of deep
453     crustal seismic anisotropy from a compilation of rock elasticity tensors and their expression in receiver functions.
454     *Tectonics* **2017**, *36*, 1835–1857. doi:10.1002/2017TC004625.
455 7.     Almqvist, B.S.; Mainprice, D. Seismic properties and anisotropy of the continental crust: Predictions based on
456     mineral texture and rock microstructure. *Reviews of Geophysics* **2017**, *55*, 367–433. doi:10.1002/2016RG000552.
457 8.     Prior, D.J.; Mariani, E.; Wheeler, J. EBSD in the Earth Sciences: Applications, Common Practice,
458     and Challenges EBSD in the Earth Sciences: Applications, Common Practice, and Challenges **2010**.
459     doi:10.1007/978-0-387-88136-2.
460 9.     Suppe, J. Geometry and Kinematics of fault-bend folding. *American Journal of Science* **1983**, *283*, 681–721.
461 10.     Smith, S.A.; Di Toro, G.; Kim, S.; Ree, J.H.; Nielsen, S.; Billi, A.; Spiess, R. Coseismic recrystallization during
462     shallow earthquake slip. *Geology* **2013**, *41*, 63–66. doi:10.1130/G33588.1.
463 11.     Busch, J.P.; van der Pluijm, B.a. Calcite textures, microstructures and rheological properties of marble mylonites
464     in the Bancroft shear zone, Ontario, Canada. *Journal of Structural Geology* **1995**, *17*, 677–688.
465 12.     Bestmann, M.; Kunze, K.; Matthews, A. Evolution of a calcite marble shear zone complex on Thassos Island,
466     Greece: Microstructural and textural fabrics and their kinematic significance. *Journal of Structural Geology* **2000**,
467     *22*, 1789–1807. doi:10.1016/S0191-8141(00)00112-7.
468 13.     Almqvist, B.S.; Hirt, A.M.; Herwegh, M.; Ebert, A.; Walter, J.M.; Leiss, B.; Burlini, L. Seismic anisotropy in the
469     Morcles nappe shear zone: Implications for seismic imaging of crustal scale shear zones. *Tectonophysics* **2013**,
470     *603*, 162–178. doi:10.1016/j.tecto.2013.05.025.

14. Barber, D.J.; Wenk, H.R.; Gomez-Barreiro, J.; Rybacki, E.; Dresen, G. Basal slip and texture development in calcite: New results from torsion experiments. *Physics and Chemistry of Minerals* **2007**, *34*, 73–84. doi:10.1007/s00269-006-0129-3.

15. Pieri, M.; Kunze, K.; Burlini, L.; Stretton, I.; Olgaard, D.L.; Burg, J.P.; Wenk, H.R. Texture development of calcite by deformation and dynamic recrystallization at 1000 K during torsion experiments of marble to large strains. *Tectonophysics* **2001**, *330*, 119–140.

16. Schuster, R.; Habler, G.; Schafler, E.; Abart, R. Microstructural and textural evolution of calcite deformed to high shear strain by high-pressure torsion. *Journal of Structural Geology* **2019**, *118*, 32–47. doi:10.1016/j.jsg.2018.09.003.

17. Schmid, S.M.; Panozzo, R.; Bauer, S. Simple shear experiments on calcite rocks: rheology and microfabrics. *J. Struct. Geol.* **1987**, *9*, 747–778.

18. Ferrero, A.M.; Migliazza, M.; Spagnoli, A.; Zucali, M. Micromechanics of intergranular cracking due to anisotropic thermal expansion in calcite marbles. *Engineering Fracture Mechanics* **2014**, *130*, 42–52. doi:10.1016/j.engfracmech.2014.01.004.

19. Lutterotti, L.; Matthies, S.; Wenk, H.R.; Schultz, a.S.J.; Richardson, J.J.W. Combined texture and structure analysis of deformed limestone from time-of-flight neutron diffraction spectra. *Journal of Applied Physics* **1997**, *81*, 594–600.

20. Leiss, B.; Molli, G. 'High-temperature' texture in naturally deformed Carrara marble from the Alpi Apuane, Italy. *Journal of Structural Geology* **2002**, *25*, 649–658.

21. Matthies, S.; Humbert, M. On the Principle of a Geometric Mean of Even-Rank Symmetric Tensors for Textured Polycrystals. *Journal of Applied Crystallography* **1995**, *28*, 254–266. doi:10.1107/S0021889894009623.

22. Punturo, R.; Kern, H.; Cirrincione, R.; Mazzoleni, P.; Pezzino, A. P- and S-wave velocities and densities in silicate and calcite rocks from the Peloritani Mountains, Sicily (Italy): The effect of pressure, temperature and the direction of wave propagation. *Tectonophysics* **2005**, *409*, 55–72. doi:10.1016/j.tecto.2005.08.006.

23. Lloyd, G.E.; Butler, R.W.H.; Casey, M.; Tatham, D.J.; Mainprice, D. Constraints on the seismic properties of the middle and lower continental crust. *From: Prior, D. J., Rutter, E. H. & Tatham, D. J. (eds) Deformation Mechanisms, Rheology and Tectonics: Microstructures, Mechanics and Anisotropy. Geological Society, London Special Publications.* **2011**, *360*, 7–32.

24. Ko, B.; Jung, H. Crystal preferred orientation of an amphibole experimentally deformed by simple shear. *Nature Communications* **2015**, *6*, 1–10. doi:10.1038/ncomms7586.

25. Debrand-Passard, S.; Courbouleix, S.; Lienhardt, M. Synthèse géologique du Sud-Est de la France: Mémoires BRGM, Orléans **1984**. pp. 1–125.

26. Courjault, T.; Grosheny, D.; Ferry, S.; Sausse, J. Detailed anatomy of a deep-water carbonate breccia lobe (Upper Jurassic, French subalpine basin). *Sedimentary Geology* **2011**, *238*, 156–171. doi:10.1016/j.sedgeo.2011.04.010.

27. BRGM. La carte géologique à 1/50000 GRENOBLE est recouverte par la coupure de la carte géologique de la France à 1/80000. *BRGM* **1970**.

28. Jourdon, A.; Rolland, Y.; Petit, C.; Bellahsen, N. Style of Alpine tectonic deformation in the Castellane fold-and-thrust belt (SW Alps, France): Insights from balanced cross-sections. *Tectonophysics* **2014**, *633*, 143–155. doi:10.1016/j.tecto.2014.06.022.

29. Gaetani, M.; Sciunnach, D.; Bini, A.; Rossi, S. Foglio 076 Lecco. Note illustrative della Carta Geologica d'Italia alla scala 1: 50.000 - ISPRA **2012**.

30. Burkhard, M. Calcite twins, their geometry, appearance and significance as stress-strain markers and indicators of tectonic regime: a review. *Journal of Structural Geology* **1993**, *15*, 351–368.

31. Ferrill, D. A., Morris, A. P., Evans, M. A., Burkhard, M., Groshong Jr, R. H., & Onasch, C.M. Calcite twin morphology: a low-temperature deformation geothermometer. *Journal of Structural Geology* **2004**, *26*, 1521–1529.

32. Passchier, C.; Trouw, R. *Microtectonics*; Vol. 275, 2005; p. 366. doi:10.1007/978-3-662-08734-3.

33. Carmignani, L.; Oggiano, G.; Barca, S.; Conti, P.; Eltrudis, A.; Funedda, A.; Pasci, S.; Salvadori, I. Memorie Descrittive Della Carta Geologica D'Italia. *Note illustrative della Carta Geologica della Sardegna a scala 1:200.000* **2001**, p. 283.

519  34.  Franceschelli, M.; Puxeddu, M.; Cruciani, G.  Variscan metamorphism in Sardinia, Italy: Review and discussion.
520      *Journal of the Virtual Explorer* **2005**, pp. 1–35.  doi:10.3809/jvirtex.2005.00121.

521  35.  Lebit, H.  On fold and strain interference patterns in the Paleozoic rocks of Iglesiente (SW Sardinia).  *Tesi di*
522      *Dottorato, ETH Zurich* **1995**.

523  36.  Carmignani, L.; Conti, P.; Funedda, A.; Oggiano, G.; Pasci, S.  La geologia della Sardegna - Geological Field
524      Tips.  *Geological Field Trips* **2012**, *4*, 104.  doi:10.3301/GFT.2012.04.

525  37.  Elter, F.M.; Corsi, B.; Cricca, P.; Muzio, G.  The south-western alpine foreland: Correlation between two sectors
526      of the variscan chain belonging to "stable Europe": Sardinia(-)Corsica and the Maures Massif (South-Eastern
527      France).  *Geodinamica Acta* **2004**, *17*, 31–40.  doi:10.3166/ga.17.31-40.

528  38.  Polino, R.; Dal Piaz, G.V.; Gosso, G.  Tectonic erosion at the Adria margin and accretionary processes for the
529      Cretaceous orogeny of the Alps. In *Deep structure of the Alps.*; Roure, F.; Heitzmann, P.; Polino, R., Eds.; Number
530      156, 1990; pp. 345–367.

531  39.  Schmid, S.M.; Haas, R.  Transition from near-surface thrusting to intrabasement decollement, Schlinig Thrust,
532      Eastern Alps.  *Tectonics Tectonics* **1989**, *8*, 697–718.

533  40.  Conti, P.; Manatschal, G.; Pfister, M.  Synrift sedimentation, Jurassic and Alpine tectonics in the central Ortler
534      Nappe, (Eastern Alps, Italy).  *Eclogae Geologicae Helvetiae* **1994**, *87*, 63–90.

535  41.  Conti, P.  The Austroalpine Ortler Nappe and the tectonic evolution of the Engadine Dolomites (Switzerland -
536      ITALY). PhD thesis, 1997.

537  42.  Berra, F.; Jadoul, F.  Stratigraphy, paleogeography and tectonic setting of the Norian succession of the Ortles
538      Nappe (Central Austroalpine, Lombardy, Northern Italy).  *Memorie di Scienze Geologiche Padova* **1999**, *51*, 78–89.

539  43.  Montrasio, A.; Berra, F.; Cariboni, M.; Ceriani, M.; Deichmann, N.; Ferliga, C.; Gregnanin, A.; Guerra, S.;
540      Guglielmin, M.; Jadoul, F.; Longhin, M.; Mair, V.; Mazzoccola, D.; Sciesa, E.; Zappone, A.  Note Illustrative dalla
541      Carta Geologica d'Italia alla scala 1:50.000 Foglio 24 CARG.  *ISPRA* **2012**, *24*, 150.

542  44.  Bigi, G.; Castellarin, A.; Coli, M.; Dal Piaz, G.V.; Sartori, R.; Scandone, P.; Vai, G.B.  Structural Model of Italy,
543      sheets 1-2, Progetto Finalizzato Geodinamica.  *CNR* **1990**.

544  45.  Piana, F.; Battaglia, S.; Bertok, C.; D'atri, A.; Ellero, A.; Leoni, L.; Martire, L.; Perotti, E.  Illite (KI) and chlorite
545      (AI) "crystallinity" indices as a constraint for the evolution of the External Briançonnais Front in Western
546      Ligurian Alps (NW Italy).  *Italian Journal of Geosciences* **2014**, *133*, 445–454.  doi:10.3301/IJG.2014.21.

547  46.  Michard, A.; Avigad, D.; Goffé, B.; Chopin, C.  The high-pressure metamorphic front of the south Western
548      Alps (Ubaye-Maira transect, France, Italy).  *Schweizerische Mineralogische und Petrographische Mitteilungen* **2004**,
549      *84*, 215–235.

550  47.  Bertok, C.; Musso, A.; D'atri, A.; Martire, L.; Piana, F.  Geology of the Colle di Tenda – monte marguareis area
551      (Ligurian Alps, NW Italy).  *Journal of Maps* **2018**, *14*, 542–551.  doi:10.1080/17445647.2018.1500497.

552  48.  Carminati, E.; Gosso, G.  Structural map of a Ligurian Briançonnais cover nappe (Conca delle Carsene, Monte
553      Marguareis, Ligurian Alps,Italy) and explanatory notes.  *Mem. Sc. Geol. Padova* **2000**, *52-1*, 93–99.

554  49.  Carminati, E.  Incremental strain analysis using two generations of syntectonic coaxial fibres: An example
555      from the Monte Marguareis Briançonnias cover nappe (Ligurian Alps, Italy).  *Journal of Structural Geology* **2001**,
556      *23*, 1441–1456.  doi:10.1016/S0191-8141(01)00010-4.

557  50.  Molli, G.; Giorgetti, G.; Meccheri, M.  Tectono-metamorphic evolution of the Alpi Apuane Metamorphic
558      Complex: New data and constraints for geodynamic models.  *Bolletino della Società Geologica Italiana* **2001**,
559      *1*, 789–800.

560  51.  Di Pisa, A.; Franceschelli, M.; Leoni, L.; Meccheri, M.  Regional variation of the metamorphic temperatures
561      across the Tuscanid I Unit and its implications on the alpine metamorphism (Apuan Alps, N-Tuscany).  *Neues*
562      *Jahrbuch für Mineralogie, Ab- handlungen* **1985**, *151*, 197–211.

563  52.  Molli, G.; Conti, P.; Giorgetti, G.; Meccheri, M.; Oesterling, N.  Microfabric study on the deformational and
564      thermal history of the Alpi Apuane marbles (Carrara marbles), Italy.  *Journal of Structural Geology* **2000**,
565      *22*, 1809–1825.

566  53.  Burlini, L.; Kunze, K.  Fabric and seismic properties of Carrara marble mylonite.  *Physics and Chemistry of the*
567      *Earth, Part A: Solid Earth and Geodesy* **2000**, *25*, 133–139.  doi:10.1016/S1464-1895(00)00022-3.

54. Carmignani, L.; Conti, P.; Disperati, L.; Fantozzi, P.; Giglia, G.; Meccheri, M. Carta Geologica del Parco delle Alpi Apuane. Scala 1:50.000, Massa. *SELCA, Firenze* **2000**.

55. Molli, G.; Vitale Brovarone, A.; Beyssac, O.; Cinquini, I. RSCM thermometry in the Alpi Apuane (NW Tuscany, Italy): New constraints for the metamorphic and tectonic history of the inner northern Apennines. *Journal of Structural Geology* **2018**, *113*, 200–216. doi:10.1016/j.jsg.2018.05.020.

56. Carmignani, L.; Conti, P.; Cornamusini, G.; Pirro, A. Geological map of Tuscany (Italy). *Journal of Maps* **2013**, *9*, 487–497. doi:10.1080/17445647.2013.820154.

57. Spalla, M.I.; Zanoni, D.; Marotta, A.M.; Rebay, G.; Roda, M.; Zucali, M.; Gosso, G. The transition from Variscan collision to continental break-up in the Alps: insights from the comparison between natural data and numerical model predictions. *Geological Society, London, Special Publications* **2014**, *405*, 363–400. doi:10.1144/SP405.11.

58. Manzotti, P.; Zucali, M. The pre-Alpine tectonic history of the Austroalpine continental basement in the Valpelline unit (Western Italian Alps). *Geological Magazine* **2013**, *150*, 153–172. doi:10.1017/s0016756812000441.

59. Zucali, M.; Manzotti, P.; Diella, V.; Pesenti, C.; Risplendente, A.; Darling, J.; Engi, M. Permian tectonometamorphic evolution of the Dent Blanche Unit (Austroalpine domain, Western Italian Alps). *Rendiconti online Società Geologica Italiana* **2011**, *15*, 133–136.

60. Roda, M.; Zucali, M.; Li, Z.X.; Spalla, M.I. Pre-Alpine contrasting tectono-metamorphic evolutions within the Southern Steep Belt, Central Alps. *Lithos* **2018**, *310-311*, 31–49. doi:10.1016/j.lithos.2018.03.025.

61. Camana, G.; Chateigner, D.; Zucali, M.; Artioli, G. The grid-work texture of authigenic microcrystalline quartz in siliceous crust-type (SCT) mineralized horizons. *American Mineralogist* **2002**, *87*, 1128.

62. Wenk, H.R. Neutron diffraction texture analysis. In *In: Neutron Scattering in Earth Sciences, Reviews in Mineralogy and Geochemistry, 63*; Mineralogical Society of America, 2006; pp. 399–426.

63. Zucali, M.; Tartarotti, P.; Capelli, S.; Ouladdiaf, B. Multiscalar structural study of the ultramafic rocks of the Antrona ophiolite (Pennine Alps). In: (Eds.) Guido Gosso, Maria Iole Spalla, and Michele Zucali, Multiscale structural analysis devoted to the reconstruction of tectonic trajectories in active ma. *Journal of The Virtual Explorer* **2012**, *41*, 1–23.

64. Zucali, M.; Chateigner, D.; Dugnani, M.; Lutterotti, L.; Ouladdiaf, B. Quantitative texture analysis of glaucophanite deformed under eclogite facies conditions (Sesia-Lanzo Zone, Western Alps); comparison between X-ray and neutron diffraction analysis. *Geological Society Special Publications* **2002**, *200*, 239–253.

65. Siegesmund, S.; Helming, K.; Kruse, R. Complete texture analysis of a deformed amphibolite: comparison between neutron, diffraction and U-stage data. *Journal of Structural Geology* **1994**, *16*, 131–142.

66. Zucali, M.; Barberini, V.; Voltolini, M.; Ouladdiaf, B.; Chateigner, D.; Mancini, L.; Lutterotti, L. Quantitative 3D microstructural analysis of naturally deformed amphibolite from the Southern Alps (Italy): Microstructures, CPO and seismic anisotropy from a fossil extensional margin. *Special Publication of The Geological Society of London* **2015**, *409*, 201–222. doi:10.1144/SP409.5.

67. Frassi, C.; Musumeci, G.; Zucali, M.; Mazzarini, F.; Rebay, G.; Langone, A. The Cotoncello Shear Zone (Elba Island, Italy): The deep root of a fossil oceanic detachment fault in the Ligurian ophiolites. *Lithos* **2017**, *278-281*, 445–463. doi:10.1016/j.lithos.2017.02.015.

68. Zucali, M.; Voltolini, M.; Ouladdiaf, B.; Mancini, L.; Chateigner, D. The 3D quantitative lattice and shape preferred orientation of a mylonitised metagranite from Monte Rosa (Western Alps): Combining neutron diffraction texture analysis and synchrotron X-ray microtomography. *Journal of Structural Geology* **2014**, *63*. doi:10.1016/j.jsg.2014.02.011.

69. Zucali, M.; Fontana, E.; Panseri, M.; Tartarotti, P.; Capelli, S.; Ouladdiaf, B. Submarine lava flow direction revealed by neutron diffraction analysis in mineral lattice orientation. *Geochemistry, Geophysics, Geosystems* **2014**, *15*. doi:10.1002/2013GC005044.

70. Frischbutter, A.; Neov, D.; Scheffzük, C.; Vrána, M.; Walther, K. Lattice strain measurements on sandstones under load using neutron diffraction. *Journal of Structural Geology* **2000**, *22*, 1587–1600. doi:10.1016/S0191-8141(00)00110-3.

71. Tartarotti, P.; Zucali, M.; Panseri, M.; Lissandrelli, S.; Capelli, S.; Ouladdiaf, B. Mantle origin of the Antrona serpentinites (Antrona ophiolite, Pennine Alps) as inferred from microstructural, microchemical, and neutron diffraction quantitative texture analysis. *Ofioliti* **2011**, *36*, 167–189.

72. Lutterotti, L.; Matthies, S.; Wenk, H.R. MAUD (Material Analysis Using Diffraction): a user friendly Java program for Rietveld Texture Analysis and more. Proceedings of the Twelfth International Conference on Textures of Materials (ICOTOM-12); Szpunar J. A.., Ed., 1999, Vol. 2, pp. 1599–1605.

73. Matthies, S.; Wenk, H.R.; Vinel, G.W. Some basic concepts of texture analysis and comparison of three methods to calculate orientation distributions from pole figures. *Journal of Applied Crystallography* **1988**, *21*, 285–304. doi:10.1107/S0021889888000275.

74. Viani, A.; Gualtieri, A.F.; Puente Orench, I.; Zucali, M. Texture analysis of magnesium potassium phosphate ceramics. *Institut Laue-Langevin (ILL)* **2016**. doi:doi:10.5291/ILL-DATA.1-02-201.

75. Zucali, M.; Capelli, S.; Chateigner, D.; Ouladiaf, B. Deep mantle related natural microstructures assessed by Quantitative Texture Analysis of natural rocks. *Institut Laue-Langevin (ILL)* **2012**. doi:10.5291/ILL-DATA.5-11-397.

76. Zucali, M.; Benitez Perez, J.; Chateigner, D.; Gomez-Barreiro, J.; Lutterotti, L.; Ouladdiaf, B. Rheology of the lower crust: Quantitative Texture Analysis of High Pressure - High Temperature rocks from Alps and Iberian Variscan belt. *Institut Laue-Langevin (ILL)* **2014**. doi:10.5291/ILL-DATA.1-02-163.

77. Babuska, V.; Cara, M. *Seismic anisotropy in the Earth*; Vol. 10, Springer, 1991.

78. Mainprice, D.; Humbert, M.; Wagner, F. Phase Transformations and Inherited ODFs Implications for Petrophysical Properties. *Textures and Microstructures* **1991**, *14*, 339–345. doi:10.1155/TSM.14-18.339.

79. Hill, R. The Elastic Behaviour of a Crystalline Aggregate. *Proceedings of the Physical Society. Section A* **1952**, *65*, 349–354. doi:10.1088/0370-1298/65/5/307.

80. Bachmann, F.; Hielscher, R.; Schaeben, H. Texture analysis with MTEX- Free and open source software toolbox. Solid State Phenomena, 2010. doi:10.4028/www.scientific.net/SSP.160.63.

81. Mainprice, D.; Hielscher, R.; Schaeben, H. Calculating anisotropic physical properties from texture data using the MTEX open-source package. *Geological Society, London, Special Publications* **2011**, *360*, 175–192. doi:10.1144/SP360.10.

82. Burlini, L.; Marquer, D.; Challandes, N.; Mazzola, S.; Zangarini, N. Seismic properties of highly strained marbles from the Splügenpass, central Alps. *Journal of Structural Geology* **1998**, *20*, 277–292. doi:10.1016/S0191-8141(97)00084-9.

83. Faccenda, M.; Bressan, G.; Burlini, L. Seismic properties of the upper crust in the central Friuli area (northeastern Italy) based on petrophysical data. *Tectonophysics* **2007**, *445*, 210–226. doi:10.1016/j.tecto.2007.08.004.

84. Brownlee, S.J.; Hacker, B.R.; Salisbury, M.; Seward, G.; Little, T.A.; Baldwin, S.L.; Abers, G.A. Predicted velocity and density structure of the exhuming Papua New Guinea ultrahigh-pressure terrane. *Journal of Geophysical Research: Solid Earth* **2011**, *116*, 1–15. doi:10.1029/2011JB008195.

85. Connolly, J.A. Multivariable phase diagrams: an algorithm based on generalized thermodynamics. *American Journal of Science* **1990**, *290*, 666–718. doi:10.2475/ajs.290.6.666.

86. pyWerami (v. 0.25) - a stand-alone program to make countour-3D plot from data file generated by the PerpleX program WERAMI or tci file generated by TCInvestigator. https://github.com/ondrolexa/pywerami/, 2017.

87. Zhang, K.J.; Li, Q.H.; Yan, L.L.; Zeng, L.; Lu, L.; Zhang, Y.X.; Hui, J.; Jin, X.; Tang, X.C. Geochemistry of limestones deposited in various plate tectonic settings. *Earth-Science Reviews* **2017**, *167*, 27–46. doi:10.1016/j.earscirev.2017.02.003.

88. Holland, T.J.B.; Powell, R. An internally consistent thermodynamic data set for phases of petrological interest. *Journal of Metamorphic Geology* **1998**, *16*, 309–344.

89. Holland, T.J.; Powell, R. An improved and extended internally consistent thermodynamic dataset for phases of petrological interest, involving a new equation of state for solids. *Journal of Metamorphic Geology* **2011**, *29*, 333–383. doi:10.1111/j.1525-1314.2010.00923.x.

90. Fisher, N.I.; Lewis, T.; Embleton, B.J. *Statistical analysis of spherical data*; Cambridge University Press, 1993; p. 329. doi:10.2307/3620138.

91.  Chateigner, D. Reliability criteria in quantitative texture analysis with experimental and simulated orientation distributions. *Journal of Applied Crystallography* **2005**, *38*, 603–611. doi:10.1107/S0021889805013695.

92.  Schaeben, H. Texture analysis of heterogeneous data–a farewell to F-coefficients. *Journal of Structural Geology* **2000**, *22*, 1565–1568.

93.  Wenk, H.R.; Takeshita, T.; Bechler, E.; Erskine, B.G.; Matthies, S. Pure shear and simple shear calcite textures. Comparison of experimental, theoretical and natural data. *Journal of Structural Geology* **1987**, *9*, 731–745. doi:10.1016/0191-8141(87)90156-8.

94.  Burlini, L.C.M.; Rutter, E.H.; Anonymous. Preferred orientation development in hot-pressed synthetic, ultrafine-grained calcite rocks. *Terra Abstracts* **1993**, *5, Suppl.*, 288.

95.  Casey, M.; Rutter, E.H.; Schmid, S.M.; Siddans, A.W.B.; Whalley, J.S. Texture development in experimentally deformed calcite rocks. *proc. 5th ICOTOM, Göttstein & Lücke (eds)* **1978**, *2*, 231–240.

96.  Trullenque, G.; Kunze, K.; Heilbronner, R.; Stünitz, H.; Schmid, S.M. Microfabrics of calcite ultramylonites as records of coaxial and non-coaxial deformation kinematics: Examples from the Rocher de l'Yret shear zone (Western Alps). *Tectonophysics* **2006**, *424*, 69–97. doi:10.1016/j.tecto.2006.06.004.

97.  Schmid, S.M.; Casey, M.; Starkey, J. The microfabric of calcite tectonites from the Helvetic Nappes (Swiss Alps). *in: Thrust and Nappe Tectonic, Geological Society of London* **1981**, pp. 151–158.

98.  Ratschbacher, L.; Wenk, H.R.; Sintubin, M. Calcite textures; examples from nappes with strain-path partitioning. *Journal of Structural Geology* **1991**, *13*, 369–384.

99.  Erskine, B.G.; Heidelbach, F.; Wenk, H.R. Lattice preferred orientations and microstructures of deformed Cordilleran marbles: correlation of shear indicators and determination of strain path. *Journal of Structural Geology* **1993**, *15*, 1189–1205. doi:10.1016/0191-8141(93)90163-5.

100. Leiss, B.; Siegesmund, S.; Weber, K. Texture Asymmetries as Shear Sense Indicators in Naturally Deformed Mono- and Polyphase Carbonate Rocks. *Textures and Microstructures* **1999**, *33*, 61–74. doi:10.1155/tsm.33.61.

101. Pieri, M.; Burlini, L.; Kunze, K.; Stretton, I.; Olgaard, D.L. Rheological and microstructural evolution of Carrara marble with high shear strain: Results from high temperature torsion experiments. *Journal of Structural Geology* **2001**, *23*, 1393–1413.

102. De Wall, H.; Bestmann, M.; Ullemeyer, K. Anisotropy of diamagnetic susceptibility in Thassos marble: A comparison between measured and modeled data. In *Journal of Structural Geology*; Leiss, B.; Ullemeyer, K.; Weber, K., Eds.; Pergamon. Oxford, International., 2000; Vol. 22, pp. 1761–1771. doi:10.1016/S0191-8141(00)00105-X.

103. Ebert, A.; Herwegh, M.; Pfiffner, A. Cooling induced strain localization in carbonate mylonites within a large-scale shear zone (Glarus thrust, Switzerland). *Journal of Structural Geology* **2007**, *29*, 1164–1184. doi:10.1016/j.jsg.2007.03.007.

104. Demurtas, M.; Smith, S.A.; Prior, D.J.; Spagnuolo, E.; Di Toro, G. Development of crystallographic preferred orientation during cataclasis in low-temperature carbonate fault gouge. *Journal of Structural Geology* **2019**, *126*, 37–50. doi:10.1016/j.jsg.2019.04.015.

105. Fernández, F.J.; Brown, D.; Álvarez-Marrón, J.; Prior, D.J.; Pérez-Estaún, A. Microstructure and lattice preferred orientation of calcite mylonites at the base of the southern Urals accretionary prism. *Journal of the Geological Society* **2004**, *161*, 67–79. doi:10.1144/0016-764903-027.

106. Parsons, A.J.; Law, R.D.; Lloyd, G.E.; Phillips, R.J.; Searle, M.P. Thermo-kinematic evolution of the Annapurna-Dhaulagiri Himalaya, central Nepal: The Composite Orogenic System. *Geochemistry, Geophysics, Geosystems* **2016**, *17*, 1511–1539. doi:10.1002/2015GC006184.

107. Wells, R.K.; Holyoke, C.W.; Newman, J.; Kronenberg, A. Lattice-preferred orientation development in experimental and natural fine-grained dolomite shear zones. *Journal of Structural Geology* **2019**, *128*, 103874. doi:10.1016/j.jsg.2019.103874.

108. Leiss, B.; Weiss, T. Fabric anisotropy and its influence on physical weathering of different types of Carrara marbles. Journal of Structural Geology, 2000, Vol. 22, pp. 1737–1745. doi:10.1016/S0191-8141(00)00080-8.

109. Barnhoorn, A.; Bystricky, M.; Burlini, L.; Kunze, K. The role of recrystallisation on the deformation behaviour of calcite rocks: Large strain torsion experiments on Carrara marble. *Journal of Structural Geology* **2004**, *26*, 885–903. doi:10.1016/j.jsg.2003.11.024.

110. Oesterling, N.; Heilbronner, R.; Stünitz, H.; Barnhoorn, A.; Molli, G. Strain dependent variation of microstructure and texture in naturally deformed Carrara marble. *Journal of Structural Geology* **2007**, *29*, 681–696. doi:10.1016/j.jsg.2006.10.007.

111. Negrini, M.; Smith, S.A.; Scott, J.M.; Tarling, M.S. Microstructural and rheological evolution of calcite mylonites during shear zone thinning: Constraints from the Mount Irene shear zone, Fiordland, New Zealand. *Journal of Structural Geology* **2018**, *106*, 86–102. doi:10.1016/j.jsg.2017.11.013.

112. De Bresser, J.H. Calcite c-axis textures along the Gavarnie thrust zone, central Pyrenees. *Geologie en Mijnbouw* **1989**, *68*, 367–375.

113. Anselmetti, F.S.; Eberli, G.P. Sonic Velocity in Carbonate Sediments and Rocks. *Carbonate Seismology* **1997**, pp. 53–74. doi:10.1190/1.9781560802099.ch4.

114. Bassinot, F.C.; Marsters, J.C.; Mayer, L.A.; Wilkens, R.H. Velocity anisotropy in calcareous sediments from Leg 130, Ontong Java Plateau. *Proc., scientific results, ODP, Leg 130, Ontong Java Plateau* **1993**. doi:10.2973/odp.proc.sr.130.041.1993.

115. Park, S.; Ishii, M. Near-surface compressional and shear wave speeds constrained by body-wave polarization analysis. *Geophysical Journal International* **2018**. doi:10.1093/gji/ggy072.

116. Cloos, M. Lithospheric buoyancy and collisional orogenesis: subduction of oceanic plateaus, continental margins, island arcs, spreading ridges, and seamounts. *Geological Society of America Bulletin* **1993**, *105*, 715–737. doi:10.1130/0016-7606(1993)105<0715:LBACOS>2.3.CO.

117. Rudnick, R.L.; Fountain, D.M. Nature and composition of the continental crust: A lower crustal perspective. *Reviews of Geophysics* **1995**, *33*, 267–309. doi:10.1029/95RG01302.